UNIVERSIDADE DE LISBOA
FACULDADE DE CIÊNCIAS
DEPARTAMENTO DE FÍSICA

Cell-mediated Self-assembly of Colloidal Scaffolds

Gonçalo Filipe Cruz Antunes

Mestrado em Física
Especialização em Física da Matéria Condensada e Nanomateriais

Dissertação orientada por:
Prof. Dr. Nuno Araújo

2018

Acknowledgements

I would like to thank Nuno Araújo first and foremost, for his wise mentoring, inexhaustible energy, and unwavering patience. I am truly grateful for the opportunities he has given me.
I would like to thank Cristóvão Dias, who has greatly helped me in many ways when producing this work, including supplying part of the code used in chapter 4. I would like to mention my office mates, André Matias and Luís Rebelo, who have provided fruitful discussions and camaraderie, as well as all of CFTC, particularly Margarida Telo da Gama, Mykola Tasinkevych, André Nunes and Diogo Pinto. Cell-mediated self-assembly is but a small fraction of the knowledge I have acquired from all of these people.
Lastly, I would like to thank my parents and my friends, without which I would not be able to finish nor start this endeavor.

Abstract

Techniques for the growth of artificial tissues often make use of a solid structure (known as scaffold) which facilitates the spontaneous growth of the tissue. Commonly, these scaffolds are produced through 3D printing which is currently unable to meet the growing demand for artificial tissues. A novel approach is to construct a system of colloidal particles that spontaneously aggregate with cells mediating the bonds. With this technique, we avoid the need of an invasive surgery as the scaffold is constructed already inside the body.

Through a set of mean-field rate equations and percolation theory, we show that suppressing the natural adhesion between cells results in larger scaffolds that self-assemble faster. Simulations of two lattice models using the kinetic Monte Carlo technique reveal how practitioners can tune the ratio of cells to particles and the ratio of diffusion coefficients to obtain desired scaffold characteristics such as size, interconnectivity, and assembly time. In particular, an optimal value of the ratio of cells to particles was found such that a larger, more interconnected scaffold assembles faster.

We show also that aggregate diffusivity is crucial for the dynamics, having studied the limits in which size does not effect diffusivity and in which diffusion of aggregates occurs on a much slower timescale than the diffusion of particles and cells. For the former, an interval of the ratio of cells to particles was found such that a giant aggregate that includes all particles forms, in agreement with some simple calculations. For the latter, it was found that the average size of aggregates exhibits a bimodal shape as a function of the ratio of cells to particles with two optimal values in the asymptotic limit. The proposed mechanism involving the suppression of bonds between a portion of the particles is verified with an analytical treatment and simulations. We show that the ratio of diffusion coefficients of cells and particles can suppress these two optimal values through two distinct mechanisms.

Keywords: linker-mediated aggregation, cell dynamics, patchy colloids, self-assembly, scaffolds.

Resumo

Técnicas para a formação de tecido artificial muitas vezes fazem uso de uma estrutura sólida (conhecida como armação) que funciona como um substituto temporário para a matriz extracelular, e facilita o crescimento espontâneo de tecido. Várias restrições são impostas sobre as armações, entre elas biocompatibilidade, biodegradabilidade e porosidade e resistência mecânica adequadas.

Commumente, estas armações são produzidas usando impressoras 3D, uma técnica que é incapaz de satisfazer a procura crescente de tecidos artificiais. A necessidade de impressão da armação fora do corpo tem associada problemas técnicos referentes à biocompatibilidade, assim como problemas económicos devido à necessidade de uma cirurgia. Uma técnica recentemente proposta consiste numa solução injetável de partículas coloidais que se auto-organizam para formar a armação desejada *in situ*, não sendo necessária uma intervenção médica invasiva. A superfície das partículas coloidais é biofuncionalizada com anticorpos que interagem selectivamente com as células que formam o tecido desejado. Células servem então de mediador das ligações entre partículas, que se agregam para formar a armação. As células mediadoras depois proliferam e formam o tecido usando a armação como âncora.

Como as ligações entre células e partículas são efectivamente irreversíveis, o balanço detalhado não é alcançado e o formalismo da física estatística de equilíbrio é incapaz de descrever adequadamente o problema. Novos modelos e técnicas foram desenvolvidos de maneira a capturar a física, que é sensível à dinâmica tanto individual como coletiva. Neste trabalho, aumentou-se a complexidade dos modelos gradualmente, permitindo o estudo detalhado do efeito de cada contribuição através de um modelo de partículas com valência limitada (*patchy*).

Numa primeira abordagem escreveu-se um sistema de equações de balanço para estudar a dinâmica das células na presença e ausência da adesão natural entre células. Definiu-se uma probabilidade de ligação entre *patches* e uma distribuição do número de ligações, ambas estudadas analiticamente e numericamente. No caso da ausência de ligações entre células, foi possível resolver as equações analiticamente para um intervalo de parâmetros e uma aproximação foi desenvolvida que recupera as soluções para outro intervalo. No caso da presença de ligações entre células, estudou-se também a dinâmica de agregados de células.

Em ambos os casos, foi descoberto que o número de células por partícula é crucial para a dinâmica, limitando o número de ligações através do defeito ou excesso de células. Encontrou-se um valor ótimo para o número de células por partícula que maximiza a probabilidade de ligação quando as ligações entre células estão ausentes. Como é preciso um *patch* com célula e outro sem célula, este valor ótimo é tal que o número de células é metade do número de *patches*. Encontrou-se também que a razão entre os coeficientes de difusão de células e partículas controla a competição entre células com uma ou nenhuma ligação pelos *patches* livres, servindo como parâmetro de controlo para a probabilidade assintótica de ligação. O coeficiente de difusão das partículas é função do seu tamanho e pode então ser ajustado para obter a armação desejada.

Comparando os dois modelos, descobriu-se que o modelo sem ligações entre células resulta em armações

maiores e mais interligadas que se auto-organizam em menos tempo. Este resultado não só tem interesse do ponto do vista teórico como permite experimentalmente produzir armações mais eficazes e menos prováveis de sofrer influências indesejadas pela bioatividade do meio envolvente. Finalmente, aplicou-se percolação de campo médio para obter o intervalo de parâmetros no qual a armação forma um gel.
Estudaram-se os efeitos das correlações espaciais entre agregados através de um modelo de rede que foi resolvido numericamente, usando-se uma variante de *kinetic* Monte Carlo com rejeições. Esta técnica baseia-se na listagem de eventos possíveis (difusão para vizinhos) e seleciona a partícula/célula que difunde com uma probabilidade proporcional à taxa de difusão de partículas/células (fixada no início da simulação e proporcional ao coeficiente de difusão).
No modelo de rede, os agregados são árvores e pontuais; o tamanho dos agregados é contabilizado através de duas probabilidades de ligação. Estudou-se em detalhe o efeito da difusividade dos agregados. O limite onde o tamanho de um agregado não tem efeito sobre a sua difusividade mostra forte dependência no número de células por partícula. Três regimes foram identificados tendo em conta o seu estado assintótico; num deles, todas as partículas formam um único agregado. Este resultado é importante para os experimentalistas pois é necessário uma armação macroscópica para se formar um tecido saudável. Um cálculo simples recupera esta partição do espaço de parâmetros usando apenas a condição de agregados serem árvores. Nos outros dois regimes, encontrou-se a forma funcional da distribuição de tamanhos dos agregados, mostrando que ela tem uma cauda exponencial e portanto um tamanho médio bem-definido. Estudou-se também o efeito da razão entre os coeficientes de difusão de células e partículas, onde se verificou que controla o estado assintótico para um dos regimes apenas.
O limite onde a difusão de agregados ocorre numa escala de tempo muito mais lenta que a de partículas e células mostra fenomenologia distinta. No limite onde células difundem muito mais rapidamente que partículas, o estado assintótico mostra um tamanho médio de agregados com forma bimodal, com dois valores ótimos do número de células por partícula não-triviais, precedido por um estado transiente com apenas um valor ótimo (correspondente ao descoberto anteriormente). Estes valores ótimos correspondem às fronteiras do intervalo do número de células por partícula em que não há partículas livres no estado assintótico. Definiu-se a distribuição de *patches* com célula dos monómeros e comprovou-se que era uma binomial. Como é necessário um *patch* com célula e um sem célula para se formar uma ligação, partículas sem *patches* com células não pode formar ligações com outras partículas com nenhum *patch* com célula. O mesmo com partículas com nenhum *patch* sem célula. A impossibilidade destas ligações leva aos máximos encontrados. Um modelo simples de campo médio reproduz a posição e altura dos máximos sem qualquer parâmetro de ajuste.
Um segundo modelo de rede foi proposto e implementado com a técnica *kinetic* Monte Carlo. Neste modelo, cada partícula ocupa um lugar de rede, permitindo o estudo do efeito da forma dos agregados. Apenas se estudou o limite dos agregados muito mais lentos que partículas. Encontrou-se a mesma forma bimodal (com um ligeiro desvio em relação ao modelo descrito anteriormente), o que permitiu concluir que a forma não é relevante para o mecanismo proposto.
Tomando o limite inverso onde monómeros difundem muito mais rápido que células, descobriu-se que os máximos desaparecem. Devido a corresponderem a mecanismos diferentes, os máximos desaparecem a valores diferentes de escalas de tempo de difusão. Um dos mecanismos surge quando as células difundem mais rapidamente que as partículas e consiste numa redução efetiva do número de células por partícula, aumentando o número de dímeros. Este mecanismo só faz desaparecer um dos máximos. O segundo máximo desaparece apenas quando as partículas difundem muito mais rapidamente que as células, limite em que dímeros e células são efectivamente estáticos quando comparados com as partículas. Devido à dificuldade de formação de ligações entre células e dímeros, o tamanho médio dos agregados diminui.

Ambos os mecanismos resultam então no aumento do número de dímeros no estado assintótico.
Estudou-se a interconectividade dos agregados através da proporção de ligações que são loops, descobrindo um valor ótimo do número de células por partícula. Este valor ótimo corresponde ao valor ótimo que maximiza o tamanho médio dos agregados no estado transiente, e é explicado usando a distribuição de *patches* com célula. Um estudo dos efeitos de tamanho finito é realizado.
Concluímos com um estudo do efeito da densidade de células e partículas. Os modelos de rede são válidos apenas no limite de densidade baixas onde encontrámos uma relação linear entre a densidade e altura dos máximos do tamanho médio dos agregados.

Palavras-chave: agregação mediada por *linkers*, dinâmica celular, colóides *patchy*, auto-organização, armações

Contents

List of Figures

Chapter 1

Introduction

In the field of tissue engineering, the use of scaffolds is a popular technique to aid in the regeneration of damaged tissues *in vivo* and to produce artificial tissues *in vitro* [2]. A scaffold is a micrometric solid structure to which healthy cells can adhere. As time passes, the cells that form bonds to the scaffold proliferate, increasing the cell population. The role of the scaffold is of an anchor, accelerating the process of tissue growth as well as defining its overall shape [3].

As the scaffold is meant as a temporary replacement for the naturally occurring extracellular matrix, it must follow several restrictions: a key characteristic in avoiding rejection is biocompatibility; cells must be able to adhere to it and function as under natural conditions; it must be biodegradable, as scaffolds are intended as temporary structures that form autonomous tissues and are eventually disassembled by the body; it must be rigid enough so as to withstand mechanical perturbations; finally it must be porous enough for both cells and nutrients to be able to penetrate the scaffold. Healthy tissue requires cell adhesion on the outskirts of the scaffold as well as inside its pores [2–8].

To grow a structure that copes with these requirements at the micrometer scale, one usually makes use of a 3D printer to create a cage-like structure which is then transplanted into the patient. There are many drawbacks regarding this method. 3D-printing such small objects is very expensive and currently not suitable for large-scale industrial production, as different types of scaffolds require entirely different production processes and equipment. Also, a scaffold produced this way must be printed in a laboratory and only afterwards be inserted into the patient [9]. This brings about many new challenges concerning the biocompatibility and structural integrity of the scaffold. The need for a surgery imposes an economical bottleneck for the widespread use of scaffolds as it is not sufficient to create scaffold production lines. Skilled labor and equipment in the form of a surgeon and a hospital are also required [2, 4, 10].

An alternative fabrication technique that would reduce the requirements has been proposed by the group of J. F. Mano, at the University of Aveiro. The idea is to functionalize the surface of chitosan particles with antibodies, selected so as to form bonds only to the cells that will make up the tissue and not to each other [1]. This procedure ensures direct bonds between particles cannot occur, instead requiring a cell as mediator. These particles are injected directly into the afflicted area, where they diffuse alongside the cells, recruiting them and forming indirect particle-particle bonds. The resulting self-assembled structure will serve as a scaffold and, having formed itself inside the body, no preparation related to transportation is needed. There is no need to manually craft the scaffold in a printer as the system spontaneously self-organizes into the desired structure. The cells mediating the bonds also proliferate, serving the dual purpose of building the tissue as well as the scaffold. Typically cell division only occurs after the scaffold is formed [1, 11].

As the typical cell-particle bond energies are much higher than the thermal energy found inside the hu-

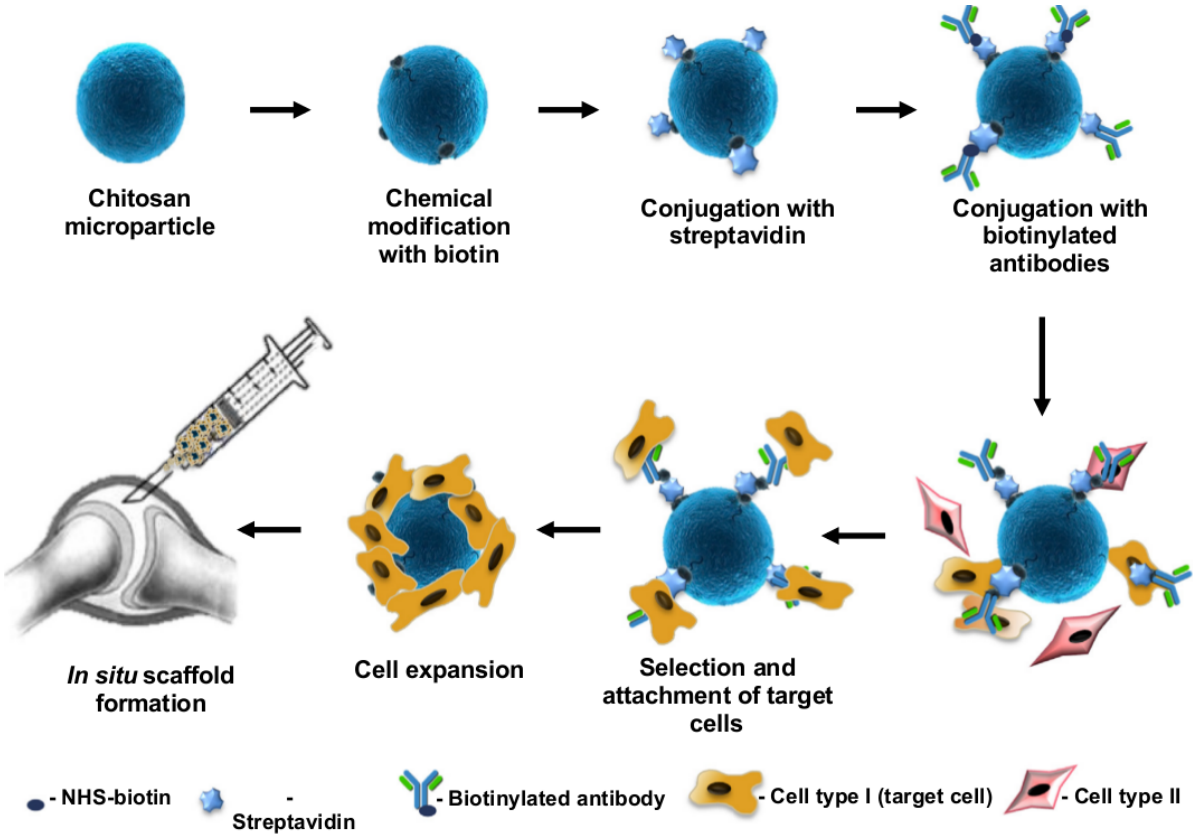

Figure 1.1: Diagram representing the preparation of self-assembling scaffolds. Chitosan microparticles are functionalized with antibodies which selectively interact with the target cells. The injectable solution forms a scaffold *in situ* [1].

man body [12], the characteristic time needed for a bond to break is much greater than the relevant experimental timescale. As the formation of bonds is effectively irreversible, detailed balance is broken and standard equilibrium statistical physics concepts and methods fail to provide an adequate description of the problem. As the system does not reach thermodynamic equilibrium, both the collective and individual dynamics are crucial for an understanding of the problem, requiring novel techniques to be developed, and making our work stand out from previous studies on aggregation with linkers [13]. Because correlations in time are important, there will be high sensitivity to variables such as concentration and diffusion coefficient of particles and cells; different models with differing degrees of complexity will be presented with the goal of characterizing the influence of each added feature. Our work can guide experiments and help to find new phenomena as theoretical studies can explore more efficiently the configuration space and isolate the effect of each separate feature of the problem.

There are many features of the experimental motivation that are physically relevant and must be included in our theoretical description. Both cells and particles are suspended in a fluid and diffuse due to microscopic collisions with the fluid molecules. Both particles and free cells can be approximated as spherical. As seen in Fig. 1.2, cells (radius $\sim 10\mu m$) are much smaller than particles (radius $\sim 100\mu m$), so their diffusion coefficient is much larger. The surface of the particles is engineered with functional groups which selectively interact with cells when they coming upon a certain distance of each other. This allows cells to mediate particle-particle bonds, which are taken to be irreversible. Due to the small size of cells when compared to the size of particles, and due to cells flattening upon adhesion [14], the case where a cell adheres to more than two particles is very unlikely, allowing us to model cells as colloidal

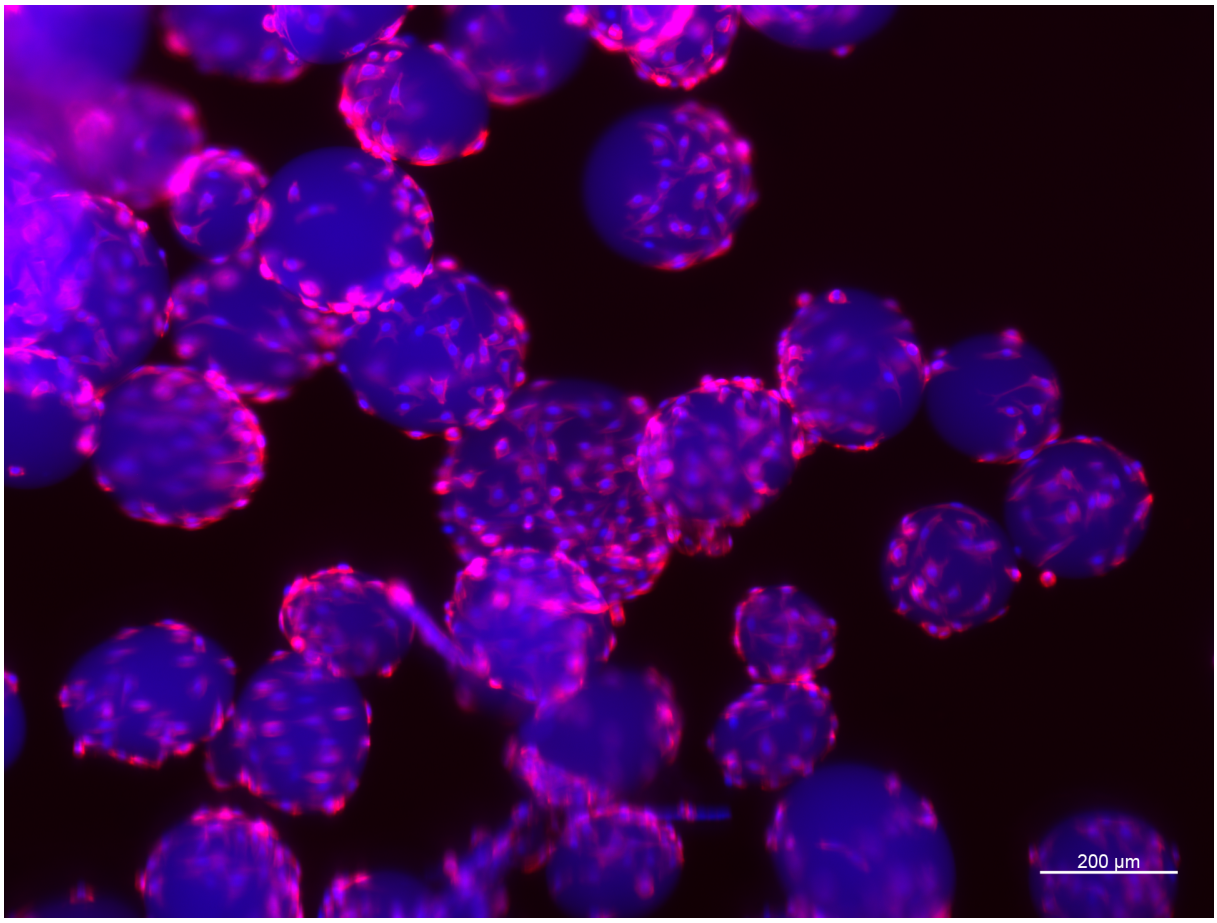

Figure 1.2: Experimental image of a self-assembled structure produced with the methodology described in Fig. (1.1). Particles in blue and cells in pink. Image courtesy of the COMPASS research group of CICECO – Aveiro Institute of Materials.

particles with two patches. The maximum coordination number a 3D compact structure of equal spheres may have is twelve [15], as seen in a cubic close-packed or an hexagonal close-packed configuration of hard spheres. The case studied in this work does not include an exterior driving force that compresses the particles together. As such, we consider particles to have only six patches, one for each direction in 3D space. The cells adhere to the antibodies which cover the surface of the particles. There are many antibodies in the surface, but only six orientations are taken to be relevant for cell-mediated bonds, consequently many cells mediate the bond between two particles. A rescaling of the cell number density, corresponding to bonds that are exclusively between one particle patch and one cell patch, greatly simplifies the model.

Cells tend to adhere to each other, a behavior that can be suppressed chemically. This suppression will not hinder tissue growth as it is not genetically encoded in the cells, and will not be inherited upon cell division. As scaffold assembly is typically much faster than cell division, only chemically treated cells take part in the process. Cell dynamics, including the effect of suppressing cell-cell bonds is studied in chapter 2 through mean-field rate equations. Chapters 3 and 4 introduce lattice models which reveal the role of correlations between aggregates and patches, respectively. Finally, some conclusions are drawn in chapter 4.

Chapter 2

Mean-field balance equations

Let us consider a system of colloidal particles and cells. The particles are spherical and their surface is functionalized with six patches. Due to the interaction of the particles with the surrounding fluid, they exhibit rotational and translational Brownian motion with diffusion coefficients D_r and D_p, respectively. As particles are much larger than the fluid molecules, there is a separation of timescales between the diffusion of fluid molecules and the one of particles, and thus the interaction with the fluid is considered uncorrelated in space and time within the timescale we are interested in. We neglect hydrodynamic interactions between particles mediated by the solvent and caused by motion-induced flow fields, which are weak at large distances between particles [16]. We instead describe the pairwise interaction between particles with an isotropic, short-range, repulsive potential.

Cells are considered isotropic and spherical, exhibiting the same translational Brownian motion as particles, but with a different diffusion coefficient. Two models will be studied for cell-cell interactions, both of which neglect hydrodynamic interactions. In the model studied in section 2.1, there is an isotropic short-range repulsion between the cells and thus cell-cell adhesion is neglected; in the model studied in section 2.2, there is an isotropic short-range attraction which mimics cell-cell adhesion.

Cells and particle patches interact with an isotropic, short-range, attractive potential, the depth of which is much lower than the thermal energy. Particles and cells form irreversible bonds as the characteristic time for bond breaking is much longer than the relevant timescale. The mechanism for aggregation is the formation of particle-particle bonds mediated by one or more cells, as direct bonds between particles cannot occur. A cell (or cell aggregate) can form a bond with two patches at most, each belonging to a different particle.

In the experimental motivation, the antibodies to which cells form bonds are much smaller than cells and are well spread-out across the surface of particles, and so cells can cover the entire surface of the particle. The maximum number of cells that can form a bond to a particle is given by σ_p/σ_c, where σ_p is the average surface area of a particle and σ_c is the average covering area of a cell after it adheres to a particle. The covering area σ_c is different than the surface area of a free cell, as cells spread on substrates upon adhesion in a highly complex way [14]. The condition of the patchy colloid model stating that patches can form bonds to only one cell is a useful simplification, as it is not necessary to consider the mediation of more than one cell since bonds are irreversible, and consequently a portion of the cells do not play a role in the dynamics. The mapping from the experimental motivation to the patchy colloid model thus implies an effective number density of cells. In the patchy colloid model, the maximum number of cells that can form a bond to a particle is f. The rescaling of the number density of cells is

thus given by

$$C_{model} = f\left(\frac{\sigma_p}{\sigma_c}\right)^{-1} C_{real}, \tag{2.1}$$

where C_{model} and C_{real} are the rescaled and the real number densities respectively. Henceforth, all references to densities correspond to the rescaled number densities instead of the real number densities in the experiments.

In this chapter, we start by studying the dynamics of the cells. We assume that the diffusion promotes a homogeneous distribution of cells and patches, such that density fluctuations in space are short-lived compared to the average time between cell-particle interactions, and that the distribution of patches is uncorrelated in space and time. Therefore, in the timescale relevant to the dynamics, densities are assumed to be constant in space (mean field). After a study of the dynamics of cells, we combine the results with mean-field percolation to study the aggregation of particles.

2.1 Without cell-cell adhesion

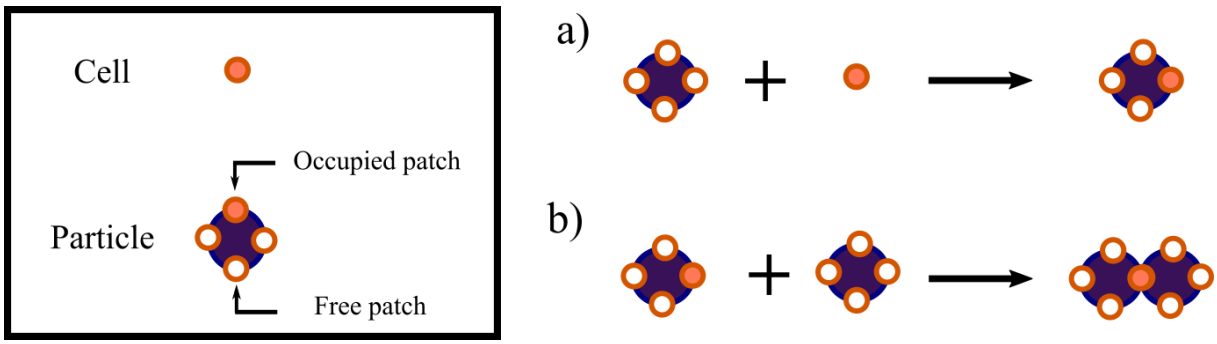

Figure 2.1: Illustration of the possible reactions when cell-cell bonds are suppressed: a) bond between a free cell and a free patch, resulting in an occupied patch; b) bond between an occupied patch and a free patch, resulting in a particle-particle bond.

We first look to the dynamics of cells when cell-cell bonds are suppressed. The only bonds that are possible are cell-particle bonds. We define $\rho(t)$ as the density of patches that do not form a bond to cells (free patches), $C_0(t)$ the density of cells that do not form a bond to patches (free cells), $C_1(t)$ the density of cells forming bonds with only one patch (occupied patches), and $C_2(t)$ the density of cells forming bonds with two patches (particle-particle bonds). We write down a set of balance equations to describe the dynamics,

$$\begin{cases} \dot{C}_0 = -k_0 C_0 \rho, & \text{(2.2a)} \\ \dot{C}_1 = k_0 C_0 \rho - k_1 C_1 \rho, & \text{(2.2b)} \\ \dot{C}_2 = k_1 C_1 \rho, & \text{(2.2c)} \\ \dot{\rho} = -k_0 C_0 \rho - k_1 C_1 \rho. & \text{(2.2d)} \end{cases}$$

C_0 (described by equation (2.2a)) always decreases as free cells form bonds with free patches and no bond is broken (see Fig. 2.1 a)). C_1 (described by eq. (2.2b)) increases with the formation of free cell-patch bonds and decreases with the formation of bonds between occupied patches and free patches (see Fig. 2.1 b)). C_2 (described by eq. (2.2c)) always increases as occupied patches form bonds with free patches and no bond may be broken. The cells act as linkers between particles, mediating particle-particle bonds. ρ (described by eq. (2.2d)) always decreases as free cells and occupied patches form bonds with free patches and no bond is broken. We have introduced two constants: k_0, which is the rate

at which free cells form bonds with free patches; and k_1, which is the rate at which occupied patches form bonds to free patches. These constants are determined by the diffusion coefficient of particles and cells. As we neglect correlations, even those in the same particle, we use the 3D coalescence reaction rate K between two species of diffusing, spherical, and isotropic particles [17, 18] in order to relate the reaction rates k_0 and k_1 with the diffusion coefficients and radii of cells and particles,

$$K = 4\pi(D_1 + D_2)(R_1 + R_2), \tag{2.3}$$

where D_1, D_2, R_1 and R_2 are the diffusion coefficients and radii of the two species respectively. Since a patch can form a bond with only one cell, we assume the radius of the patches is of the same order as the radius of the cells. The diffusion coefficients of spherical isotropic particles D_i depend on their radius R_i, as predicted by the Stokes-Einstein relation [19]

$$D_i = \frac{k_B T}{8\pi\eta\, R_i}, \tag{2.4}$$

where η is the viscosity of the suspending medium and T is the thermostat temperature. Since cells are one order of magnitude smaller than the particles, we may approximate the diffusion coefficient of occupied patches by the diffusion coefficient of particles. Using eqs. (2.3) and (2.4):

$$k_0 = 4\pi(D_c + D_p)(R_c + R_c) = \frac{k_B T}{\eta}\left(1 + \frac{R_c}{R_p}\right), \tag{2.5a}$$

$$k_1 = 4\pi(D_p + D_p)(R_c + R_c) = 2\frac{k_B T}{\eta}\frac{R_c}{R_p}, \tag{2.5b}$$

with D_c and R_c referring to cells and D_p and R_p referring to particles. We introduce k

$$k = \frac{k_1}{k_0}, \tag{2.6}$$

which is the relative rate at which occupied patches and free patches form bonds in comparison to free cells and free patches. From eqs. (2.5a) and (2.5b)

$$k = \frac{2}{1 + \frac{R_p}{R_c}}. \tag{2.7}$$

Note that $k \in]0, 2[$. If $k < 1$, particles are larger than cells; if $k > 1$, cells are larger than particles. In the experiments $R_p \approx 10R_c$ ($k \approx 0.1$), and so we are interested in the case $k < 1$. We rescale time ($t \to k_0 t$) and choose units of volume such that the system occupies unitary volume, obtaining:

$$\begin{cases} \dot{C}_0 = -C_0\rho, & \text{(2.8a)} \\ \dot{C}_1 = C_0\rho - kC_1\rho, & \text{(2.8b)} \\ \dot{C}_2 = kC_1\rho, & \text{(2.8c)} \\ \dot{\rho} = -C_0\rho - kC_1\rho. & \text{(2.8d)} \end{cases}$$

The rate constant k_0 therefore sets the timescale and k determines the dynamics. k is a major control parameter as it sets the competition for free patches between free cells and occupied patches. Increasing k increases the rate of formation of occupied patch/free patch bonds in relation to free cell/free patch

bonds.

As initial conditions, we assume that all cells and particles are free and uniformly distributed. We define n as the density of particles and f as the number of patches per particle, thus

$$\rho(0) = nf. \tag{2.9}$$

As discussed previously, we take $f = 6$ hereafter. We also introduce ϕ, which is defined as the ratio between free cells and free patches in the initial state,

$$\phi = \frac{C_0(0)}{\rho(0)}, \tag{2.10}$$

and,

$$C_0(0) = C, \tag{2.11}$$
$$C_1(0) = 0, \tag{2.12}$$
$$C_2(0) = 0, \tag{2.13}$$
$$\rho(0) = \frac{C}{\phi}. \tag{2.14}$$

Figure 2.2 shows the numerical solution of eqs. (2.8a)–(2.8d). If $\phi < 0.5$, there are enough patches for all cells to form two bonds ($C_2(\infty) = C$), as seen in Fig. 2.2 a). Since $k \ll 1$, there is a separation of timescales: the time needed for cells to form one bond is much smaller than the time needed for them to form a second bond, leading to the prolonged tail in C_1. If $\phi > 0.5$, the dynamics cease when all free patches form a bond ($\rho(\infty) = 0$), as in Fig. 2.2 b). In this case, $C_0(\infty)$, $C_1(\infty)$, and $C_2(\infty)$ depend on k. If $k \ll 1$, free cells are much faster than occupied patches, exhausting all patches before occupied patches can become particle-particle bonds $\big(C_1(\infty) > C_0(\infty)\big)$. If $k = 1$, as in Fig. 2.2 c), the two rates are the same and the two reactions compete. Eventually, the total rate of free cells turning into occupied patches equals the one of occupied patches turning into particle-particle bonds and $\dot{C}_1(t) = 0$.

Combining eqs. (2.8a)–(2.8c), we get a conservation equation for cells:

$$\dot{C}_0 + \dot{C}_1 + \dot{C}_2 = 0 \Leftrightarrow C_0 + C_1 + C_2 = C, \tag{2.15}$$

where C is the total density of cells, which is constant. Combining eqs. (2.8a), (2.8b), and (2.8d), we get a conservation equation for patches:

$$\dot{\rho} = \dot{C}_1 + 2\dot{C}_0 \Leftrightarrow \rho - C_1 - 2C_0 = \rho_0, \tag{2.16}$$

with ρ_0 being a constant. If $C < \rho(0)$, the dynamics ceases when all cells have two bonds, $C_0 = C_1 = 0$ and $\rho = \rho_0$. ρ_0 is the density of free patches after all cells form two bonds. If $\rho_0 < 0$, there are not enough patches for all cells to form two bonds and dynamics saturate due to a lack of patches rather than a lack of cells. From eqs. (2.12)–(2.14) and (2.16), we obtain

$$\rho_0 = \frac{1 - 2\phi}{\phi} C. \tag{2.17}$$

We can combine eqs. (2.8a) and (2.8b) to obtain an equation for C_1 as function of C_0 (this is possible

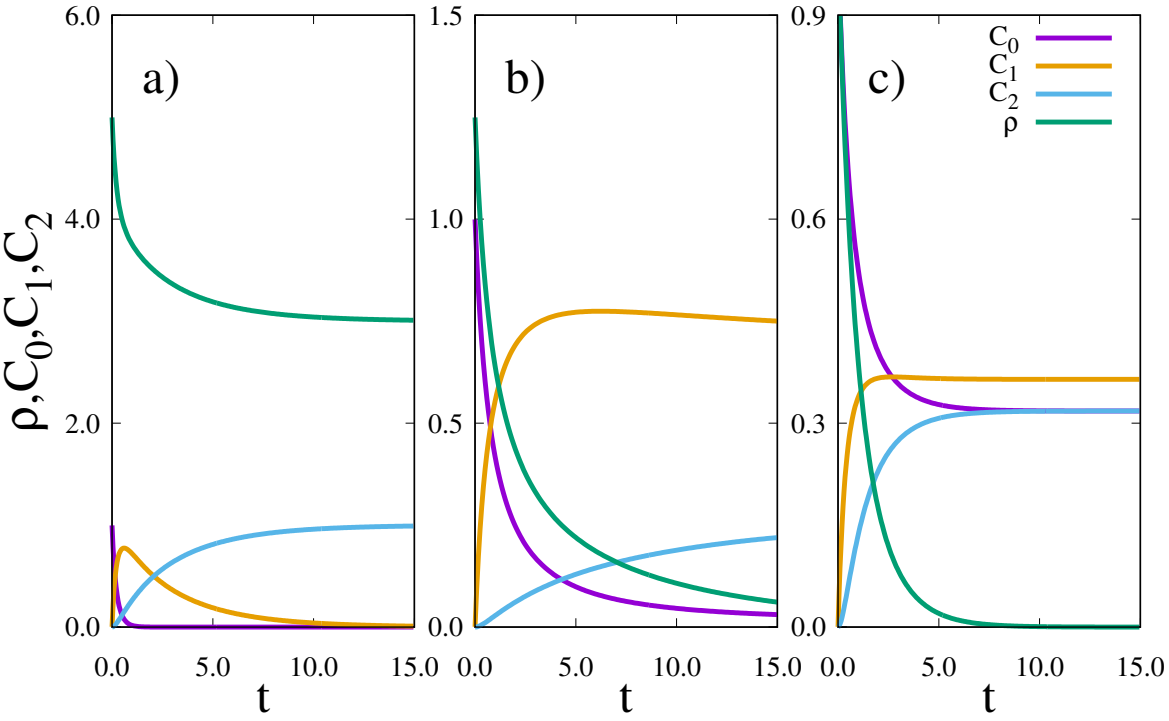

Figure 2.2: Numerical solutions of equations (2.8a)–(2.8d) for $C = 1$. Other parameters are a) $k = 0.1$, $\phi = 0.2$; b) $k = 0.1$, $\phi = 0.8$; c) $k = 1.0$, $\phi = 1.0$.

because $C_0(t)$ is injective).

$$\frac{\dot{C}_1(t)}{\dot{C}_0(t)} = \frac{dC_1}{dC_0} = k\frac{C_1}{C_0} - 1. \tag{2.18}$$

Solving this differential equation, we obtain

$$C_1 = A_1 C_0^k + \frac{C_0}{k-1} \quad \text{if } k \neq 1, \tag{2.19}$$

$$A_1 = \frac{C^{1-k}}{1-k}. \tag{2.20}$$

From (2.16) and (2.19), we obtain ρ as function of C_0:

$$\rho = A_1 C_0^k + \frac{2k-1}{k-1} C_0 + \rho_0. \tag{2.21}$$

From eqs. (2.15) and (2.19), we obtain C_2 as function of C_0:

$$C_2 = C - \left(A_1 C_0^k + \frac{k}{k-1} C_0 \right). \tag{2.22}$$

To obtain C_0 as function of time, we combine eq. (2.21) with eq. (2.8a)

$$\dot{C}_0 = -\left(A_1 C_0^{1+k} + \frac{2k-1}{k-1} C_0^2 + \rho_0 C_0 \right). \tag{2.23}$$

Solving eq. (2.23) is difficult because of the term with exponent $1 + k$, we look for ways to approximate a solution in the case of small k, which corresponds to the experiments where the cells are much smaller

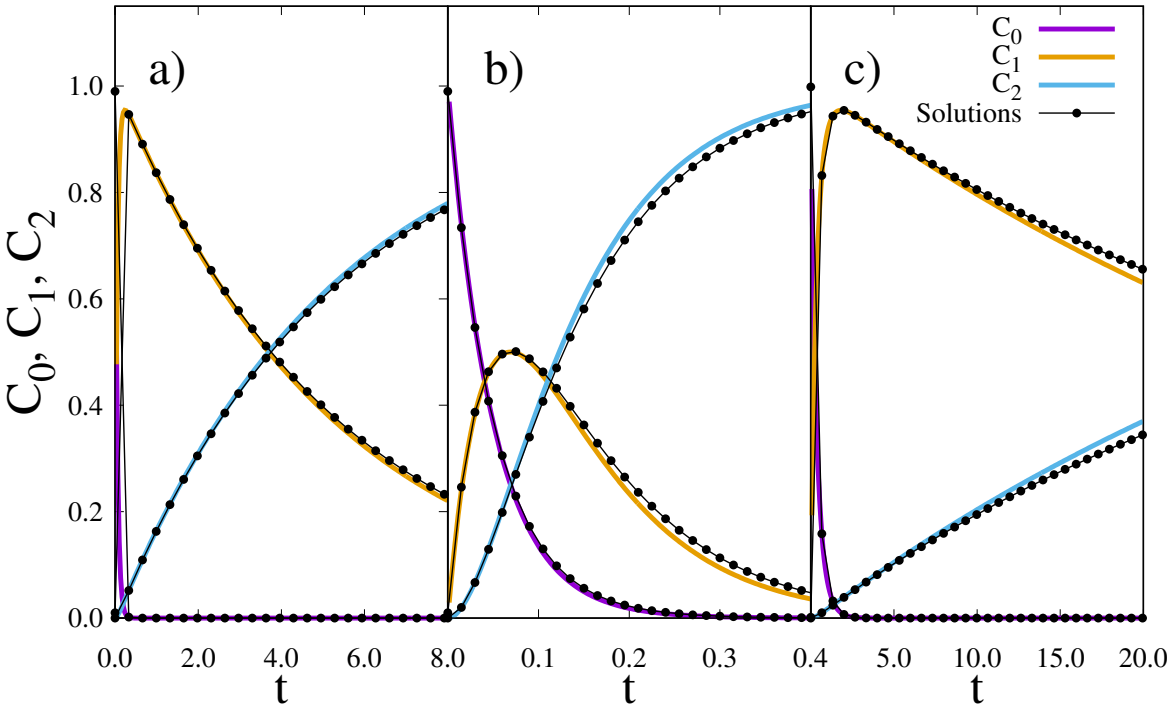

Figure 2.3: Comparison between the approximation of eq. (2.25) with the numerical solution of eqs. (2.8a)–(2.8d) (in black). $C = 1$, other parameters are a) $k = 0.01$, $\phi = 0.05$; b) $k = 0.5$, $\phi = 0.05$; and c) $k = 0.01$, $\phi = 0.3$.

than the particles. The first solvable approximation that could be tried is to ignore the k in the exponent as it is smaller than one.

$$\dot{C}_0 = -\left[(A_1 + \rho_0)C_0 + \frac{2k-1}{k-1}C_0^2\right]. \tag{2.24}$$

Defining $\gamma_1 = A_1 + \rho_0$ and $\gamma_2 = \frac{2k-1}{k-1}$ we get:

$$C_0 = \frac{\gamma_1 \ \exp(\gamma_1 \ A_2)}{\exp(\gamma_1 \ t) - \gamma_2 \exp(\gamma_1 \ A_2)}, \tag{2.25}$$

where A_2 is a constant. If $C_0(0) = C$ then

$$A_2 = \frac{1}{\gamma_1}\log\left(\frac{C}{C\gamma_2 + \gamma_1}\right). \tag{2.26}$$

It can be shown that performing a Taylor expansion on the term with exponent $1 + k$ of eq. (2.23) does not significantly improve the approximation and only introduces corrections to γ_1 and γ_2. To obtain the limits in which eq (2.25) is a valid approximation, we rearrange eq. (2.23) as

$$\dot{C}_0 = -\left((A_1 C_0^k + \rho_0)C_0 + \frac{2k-1}{k-1}C_0^2\right). \tag{2.27}$$

Expanding the exponential (keeping up to the first order term) we get

$$\dot{C}_0 = -\left\{\Big[A_1\big[1 + k\log(C_0)\big] + \rho_0\Big]C_0 + \frac{2k-1}{k-1}C_0^2\right\}. \tag{2.28}$$

If

$$A_1 + \rho_0 >> A_1 k \log(C_0), \tag{2.29}$$

we may ignore the term with the logarithm. Condition (2.29) (and thus the approximation) is valid for small values of ϕ and k (see Fig. 2.3).

The case $k = \frac{1}{2}$ in eq. (2.23) is analytically solvable. Note that $A_1 = 2C^{1/2}$. Equation (2.23) reduces to

$$\dot{C}_0 = -\left(A_1 C_0^{\frac{3}{2}} + \rho_0 C_0\right), \tag{2.30}$$

which has the solution,

$$C_0(t) = \begin{cases} \dfrac{\rho_0^2}{\left[A_1 + A_3 \exp(\frac{\rho_0 t}{2})\right]^2} & \text{if } \rho_0 \neq 0, \quad (2.31) \\ \dfrac{4}{(A_1 t + A_3)^2} & \text{if } \rho_0 = 0. \quad (2.32) \end{cases}$$

Introducing the initial conditions (and using the fact that $C_0(t)$ is strictly decreasing):

$$A_3 = \begin{cases} -\rho_0 C^{-1/2} - A_1 & \text{if } \rho_0 \neq 0, \\ 2C^{-1/2} & \text{if } \rho_0 = 0. \end{cases}$$

For the condition $\phi > \frac{1}{2}$, the dynamics cease when $\rho = 0$. Therefore we can obtain from eq. (2.21)

$$\frac{C_0(\infty)}{C} = \left(\frac{1-2\phi}{2\phi}\right)^2, \tag{2.33}$$

and from eq. (2.22)

$$\frac{C_2(\infty)}{C} = 1 + \frac{1-2\phi}{\phi} + \left(\frac{1-2\phi}{2\phi}\right)^2. \tag{2.34}$$

To characterize the self-assembled structure, we look to the bond probability p_b, defined as the probability that a patch forms a cell-mediated bond to another patch. This probability is a measure of how well-connected the structure is, as it determines the average number of cell-mediated bonds per particle. In section 2.4, the influence of p_b on the structure is discussed in more detail. p_b is given, in the thermodynamic limit, by the fraction of patches involved in indirect particle-particle bonds. As there are two involved patches per particle-particle bond, this fraction is given by

$$p_b(t) = \frac{2C_2(t)}{\rho(0)} = 2\phi\frac{C_2}{C}. \tag{2.35}$$

For $\phi \leq \frac{1}{2}$, as all cells form two bonds in the final state, we obtain

$$p_b(\infty) = 2\phi \, , \phi \leq \frac{1}{2}, \tag{2.36}$$

which is independent of k. The general case is solved numerically and the results are shown in Fig. 2.4. The predicted linear regime can be seen in Fig. 2.4 a). For $\phi > 0.5$ there are not enough patches for all cells to form two bonds. Competition between free cells and occupied patches arises and is tunable through k. As $k = k_1/k_0$ increases, the rate of occupied patches turning into particle-particle bonds

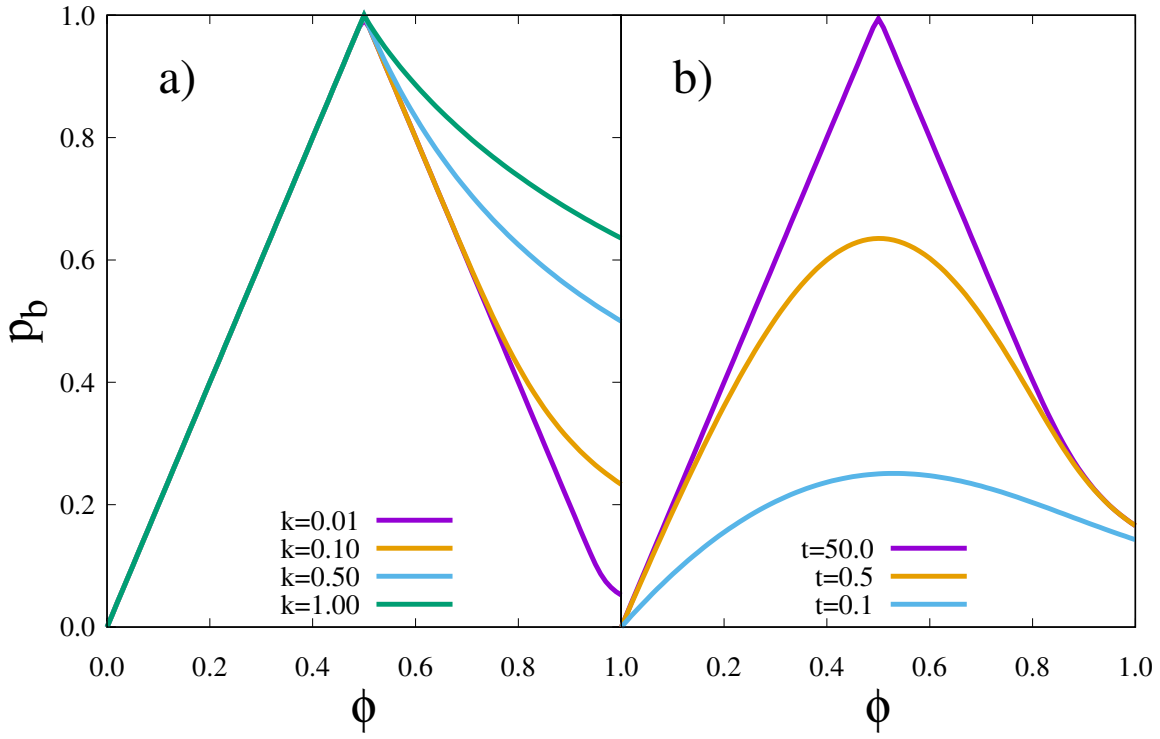

Figure 2.4: a) Asymptotic value of the probability that a patch forms a cell-mediated bond with another patch as function of ϕ for different values of k; b) Value of the probability that a patch forms a cell-mediated bond with another patch as function of ϕ for different values of time. Parameters are $\rho(0) = 14064$, $k_0 = 9 \times 10^{-3}$ and $k_1 = 5 \times 10^{-4}$, resulting in a value of $k = 5.6 \times 10^{-2}$.

increases in relation to free cells turning into occupied patches. Consequently, there are more particle-particle bonds in the final state. The limit $k \to 0$ corresponds to all free cells forming bonds before any occupied patch can find a free patch. The asymptotic p_b is thus symmetric with respect to $\phi = 0.5$,

$$\lim_{k\to 0} p_b(\infty) = \begin{cases} 2 - 2\phi & , \frac{1}{2} \leq \phi \leq 1, \quad (2.37a) \\ 0 & , 1 \leq \phi. \quad (2.37b) \end{cases}$$

The limit $k \to \infty$ corresponds to occupied patches forming bonds with free patches as soon as they are formed. In the asymptotic state, p_b is maximized for $\phi = 0.5$, which is also the case where p_b grows the fastest, as seen in Fig. 2.4 b).

The probability that a patch forms a cell-mediated bond with another patch depends on both k and ϕ. The size and density of cells are system dependent. The ratio of cells to patches ϕ can be controlled by adjusting the density of particles in the injectable solution. The ratio of rate constants k can be controlled by adjusting the radius of the particles, which we manufacture in the lab. It was also shown that the time needed for the scaffold to assemble can be fine-tuned, further showcasing the versatility of this method and the richness of its dynamics.

2.2 With cell-cell adhesion

Let us now consider the case where cells can adhere to each other. Thus, multiple cells can adhere to the same patch and aggregates composed only of cells that have not formed bonds to any patch are possible. Cell-cell adhesion is taken to be irreversible. We keep the definition of $\rho(t)$ as the density of free patches,

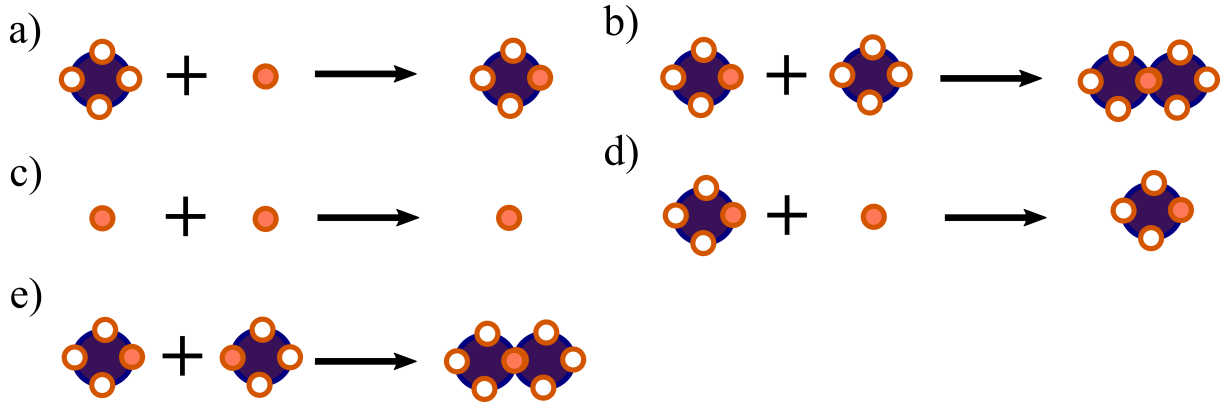

Figure 2.5: Illustration of the possible reactions when cell-cell bonds are allowed: a) Bond between a free cell/cell aggregate and a free patch, resulting in an occupied patch; b) bond between an occupied patch and a free patch, resulting in a particle-particle bond; c) bond between free cells/cell aggregates, effectively decreasing C_0; d) bond between an occupied patch and a free cell/cell aggregate; e) bond between occupied patches, resulting in a particle-particle bond.

however $C_0(t)$ is now the density of free cells and cell aggregates not forming a bond to a patch, $C_1(t)$ is the density of patches that form a bond to at least one cell (occupied patches), and $C_2(t)$ the density of bonds between two patches (mediated by one or more cell). Of importance is the fact that $C_0 + C_1 + C_2$ is not conserved. As cells are much smaller than particles, we consider that cell aggregates have the same radius and the same diffusion coefficient as a single cell. C_0 is thus the sum of the densities of free cells and cell aggregates, and C_1 is the effective density of occupied patches. The equations are as follows:

$$\begin{cases} \dot{C}_0 = -k_0 C_0 \rho - k_0 C_0 C_1 - \frac{1}{2} k_2 C_0^2, & \text{(2.38a)} \\ \dot{C}_1 = k_0 C_0 \rho - k_1 C_1 \rho - k_1 C_1^2, & \text{(2.38b)} \\ \dot{C}_2 = k_1 C_1 \rho + \frac{1}{2} k_1 C_1^2, & \text{(2.38c)} \\ \dot{\rho} = -k_0 C_0 \rho - k_1 C_1 \rho. & \text{(2.38d)} \end{cases}$$

All terms in eqs. (2.2a)–(2.2d) appear in eqs. (2.38a)–(2.38d) (see Fig. 2.5 a) and b)), with more terms being included as new mechanisms are present. The second term in (2.38a) accounts for the adhesion of multiple cells to the same patch (see Fig. 2.5 d)) and the third term accounts for the formation of cell aggregates (effectively removing free cells, see Fig. 2.5 c)). The factor of $\frac{1}{2}$ comes from the fact that two cell aggregates/free cells merge to form a larger cell aggregate. The third term in eq. (2.38b) and the second term in eq. (2.38c) reflect the possibility of forming bonds between occupied patches (mediated by one or more cells, see Fig. 2.5 e)). The factor of $\frac{1}{2}$ comes from the fact that, for every two occupied patches that form a bond, only one particle-particle bond is formed.

The rates k_0 and k_1 are given by eqs (2.5a) and (2.5b); k_2 is the reaction rate of cell aggregates/free cells with themselves and it is not independent of k_0 and k_1:

$$k_2 = 4\pi(D_c + D_c)(R_c + R_c) = 2\frac{k_B T}{\eta} = 2k_0 - k_1. \quad \text{(2.39)}$$

Rescaling time ($t \to k_0 t$), and using eq. (2.39), we get:

$$\begin{cases} \dot{C}_0 = -C_0\rho - kC_0C_1 - \dfrac{2-k}{2}C_0^2, & \text{(2.40a)} \\ \dot{C}_1 = C_0\rho - kC_1\rho - kC_1^2, & \text{(2.40b)} \\ \dot{C}_2 = kC_1\rho + \dfrac{k}{2}C_1^2, & \text{(2.40c)} \\ \dot{\rho} = -C_0\rho - kC_1\rho. & \text{(2.40d)} \end{cases}$$

Allowing cell-cell adhesion (bonds) means that even two occupied patches can form cell-mediated bonds, and that increasing ϕ cannot decrease the density of particle-particle bonds. We may obtain an estimation for $p_b(\phi)$ in the fast cell limit ($D_c \gg D_p$) if we neglect cell aggregation (and thus dropping out the third term in eq. (2.40a)). Let P be the total number of patches and C be the total number of cells. In the fast cell limit one can split the dynamics into two timescales: one where only cells diffuse and one where only particles diffuse. After the first regime, the probability p_0 that a patch does not form a bond to any cell after randomly assigning C cells to all patches is

$$p_0 = \left(\frac{P-1}{P}\right)^C, \tag{2.41}$$

where we neglected correlations between patches and distributed cells uniformly. In the thermodynamic limit (infinite system)

$$\lim_{P\to\infty} p_0 = e^{-\phi}. \tag{2.42}$$

In the second regime, occupied patches form cell-mediated bonds with other free or occupied patches. In order to calculate the number of free patches after the second regime, we construct a system of rate equations. Let ρ_0 be the number of free patches and ρ_1 be the number of occupied patches. Then,

$$\begin{cases} \dot{\rho_0} = -Q\rho_0\rho_1 & \text{(2.43a)} \\ \dot{\rho_1} = -Q\rho_0\rho_1 - Q\rho_1^2, & \text{(2.43b)} \end{cases}$$

where Q is a constant reaction rate. The initial conditions are

$$\begin{cases} \rho_0(0) = \rho p_0 & \text{(2.44a)} \\ \rho_1(0) = \rho(1-p_0). & \text{(2.44b)} \end{cases}$$

We have solved this system of equations to obtain the asymptotic value of ρ_0. In this limit, the value of Q is irrelevant.

$$\rho_0' = \lim_{t\to\infty} \rho_0 = \rho \exp[1 - \exp(\phi) - \phi]. \tag{2.45}$$

We can now calculate p_b:

$$p_b = \frac{\rho - \rho_0'}{\rho} = 1 - \exp[1 - \phi - \exp(\phi)]. \tag{2.46}$$

As can be seen in Fig. 2.6 a), the approximation of neglecting cell aggregates of eq. (2.46) predicts higher values of p_b than the ones obtained numerically from solving eqs. (2.40a)–(2.40d). This is because cell aggregates effectively reduce the number of possible particle-particle bonds. There is better agreement for low values of ϕ.

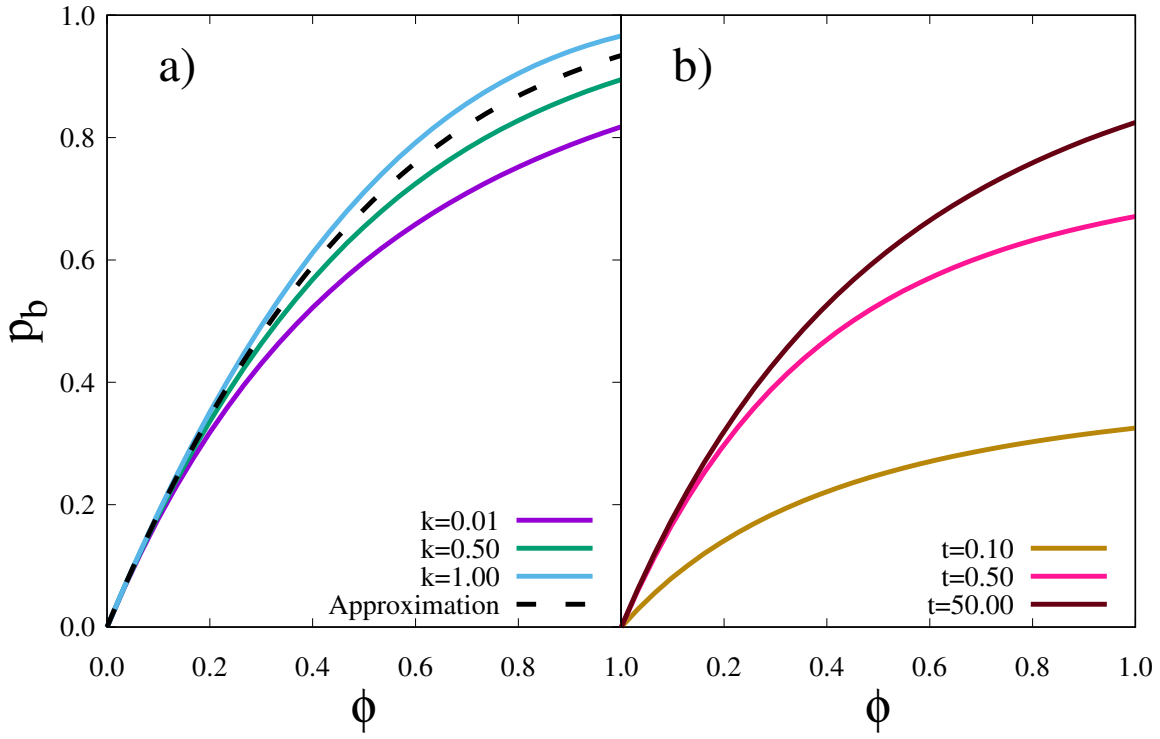

Figure 2.6: a) Asymptotic value of the probability that a patch forms a cell-mediated bond with another patch as function of ϕ for different values of k. The dashed line represents the approximation obtained in eq (2.46). b) Value of the probability that a patch forms a cell-mediated bond with another patch as function of ϕ for different values of time. $\rho(0) = 14064$, $k_0 = 9 \times 10^{-3}$ and $k_1 = 5 \times 10^{-4}$, resulting in a value of $k = 5.6 \times 10^{-2}$.

In order to study the effects of cell aggregation, we split eq. (2.38a) into two equations. One equation describes the density of free cells C_f, and the other describes the density of cell aggregates C_c. The two are such that $C_f + C_c = C_0$. As for eqs. (2.2a)–(2.2d) and (2.38a)–(2.38d),

$$\begin{cases} \dot{C}_f = -k_0 C_f \rho - k_1 C_f C_1 - k_2 C_f^2 - k_2 C_f C_c, & \text{(2.47a)} \\ \dot{C}_c = -k_0 C_c \rho - k_1 C_c C_1 + \frac{1}{2} k_2 C_f^2 - \frac{1}{2} k_2 C_c^2. & \text{(2.47b)} \end{cases}$$

The first two terms in eqs. (2.47a) and (2.47b) relate to free cells and cell aggregates forming bonds with free and occupied patches, respectively (see Fig. 2.7 a)-d)). The third term in eqs. (2.47a) and (2.47b) refers to the formation of cell aggregates (see Fig. 2.7 e)). Cell aggregates grow by capturing other cell aggregates and free cells, as reflected in the fourth term in eqs. (2.47a) and (2.47b) (see Fig. 2.7 f) and g)).

While both C_c and C_f tend to zero, the proportion of C_0 in the form of cell aggregates saturates to a constant value that depends on ϕ (see Fig. 2.8). The ratio increases as ϕ increases, as there are less patches per cell, being more likely for free cells to find each other before they find free patches. The ratio decreases with k; as free cells diffuse slower in relation to particles, it is less likely that free cells find each other before finding a free patch.

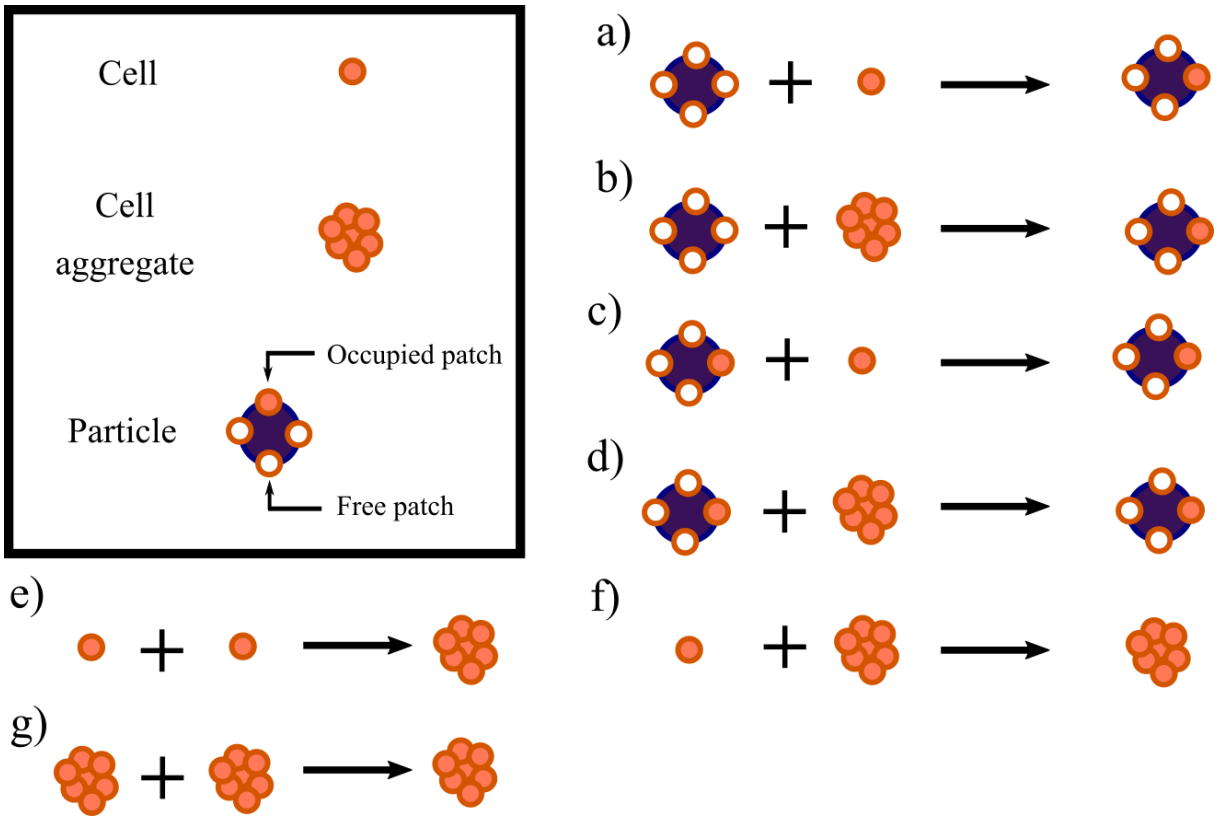

Figure 2.7: Illustration of the possible reactions when cell-cell bonds are allowed. a),b) Bonds between a free patch and a free cell/cell aggregate, resulting in a occupied patch; c), d), e), f), g) bonds between cells, effectively decreasing C_0.

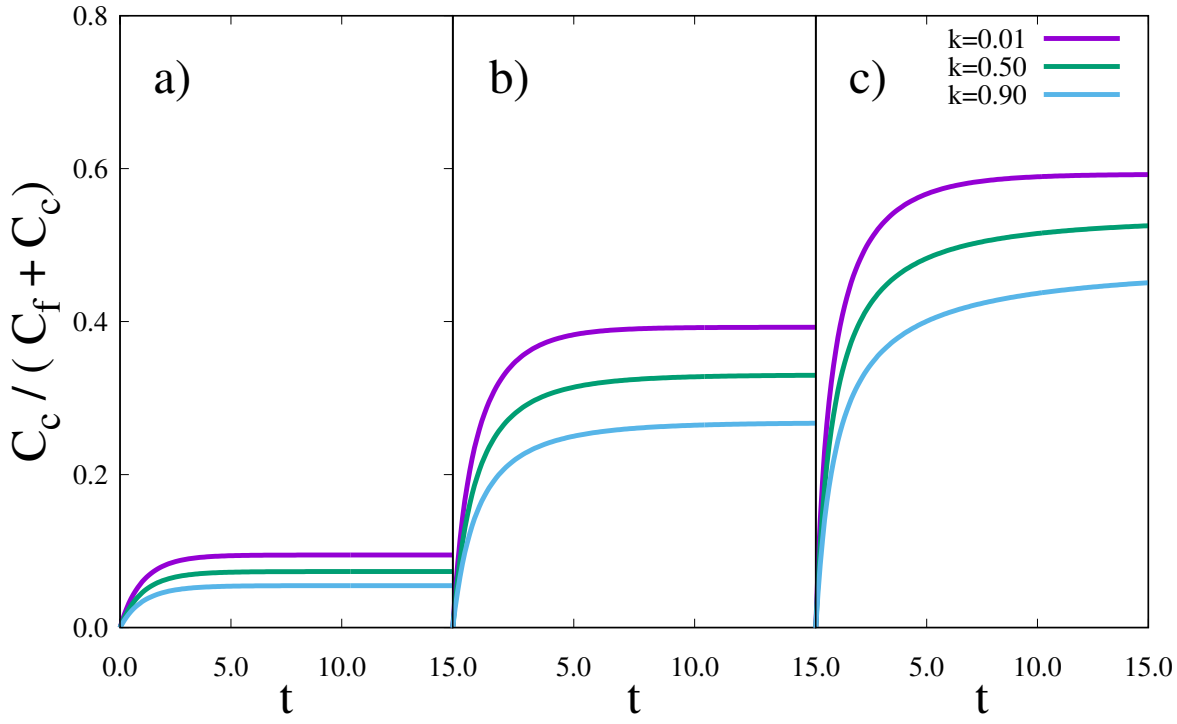

Figure 2.8: Value of the proportion of cell aggregates as a function of time for different values of k. Parameters are $k_0 = 1$, $\rho(0) = 1$, and $\phi = \{0.1, 0.5, 0.9\}$ for a), b), and c), respectively.

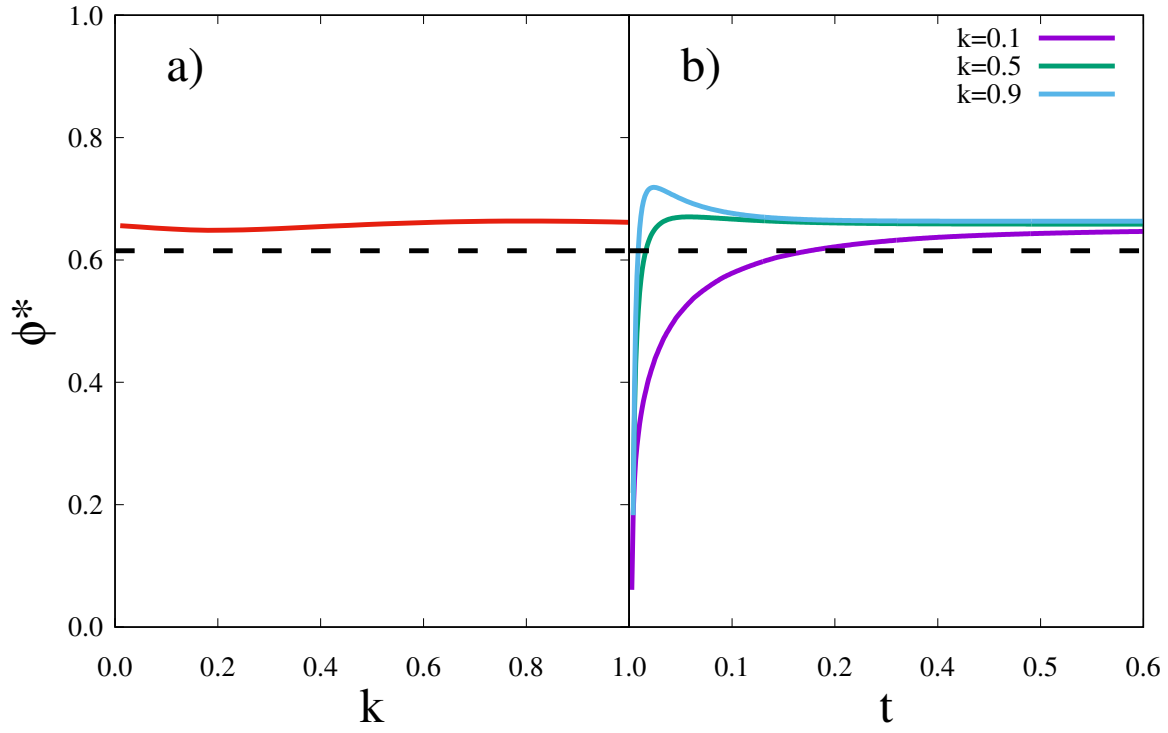

Figure 2.9: a) Asymptotic value of ϕ^* as function of k. The dashed line represents the approximation obtained in (2.46). b) Value of ϕ^* as function of time for different values of k. $\rho(0) = 14064$, $k_0 = 9 \times 10^{-3}$.

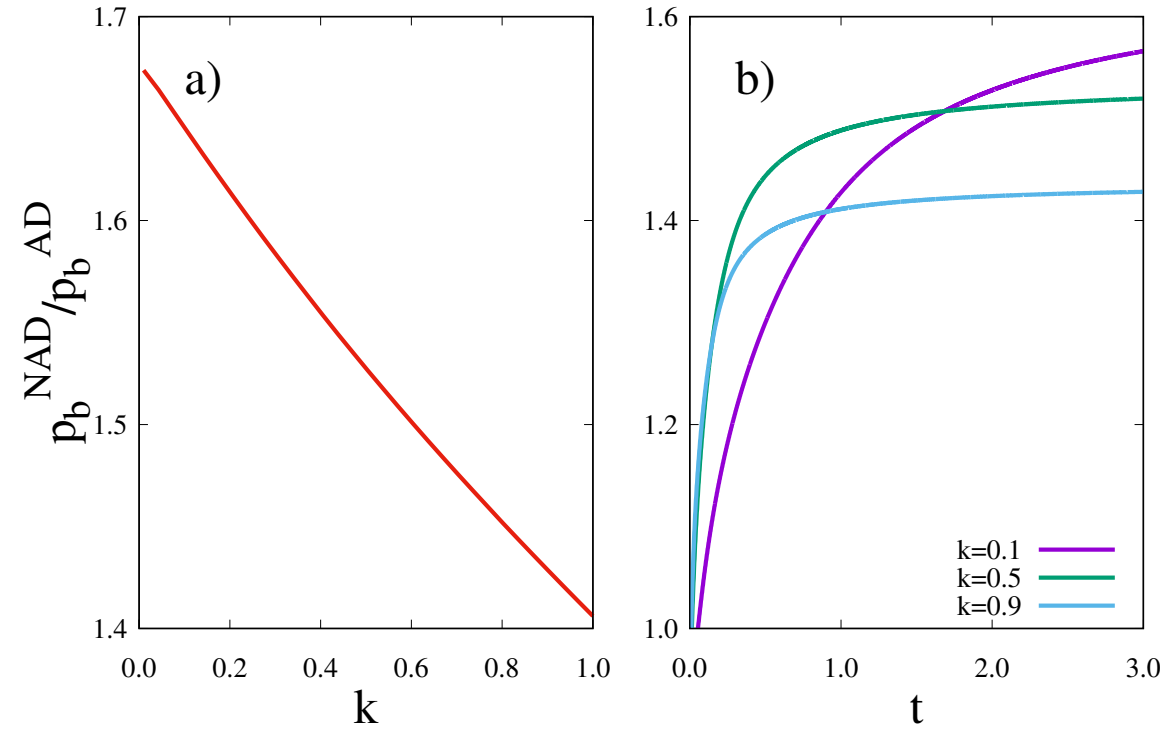

Figure 2.10: a) Asymptotic gain in p_b for $\phi = 0.5$. p_b^{NAD} is the bond probability obtained when cell-cell adhesion is suppressed, while p_b^{AD} is the bond probability obtained otherwise; b) value of the bond probability gain as function of time for different values of k. $\rho(0) = 14064$, $k_0 = 9 \times 10^{-3}$.

2.3 Comparison between the two mechanisms

We now compare the two mechanisms in order to determine if suppressing cell-cell adhesion is an advantage for scaffold production. We have found that suppressing cell-cell adhesion results in higher values of p_b for values of ϕ lower than some threshold value $\phi^*(t)$, meaning that less cells are required in order to obtain the same bond probability. When allowing cell adhesion, many cells form cell aggregates and/or adhere to occupied patches, and so not every cell is used for forming bonds between particles, effectively lowering the value of ϕ as some are redundant. The threshold ratio of cells to patches $\phi^*(\infty)$ in the fast cell limit can be approximated using eqs. (2.37a), where we neglect cell aggregates, and eq. (2.46). The approximated $\phi^*(\infty)$ is such that

$$1 - 2\phi^*(\infty) + \exp\left\{1 - \phi^*(\infty) - \exp\left[\phi^*(\infty)\right]\right\} = 0, \tag{2.48}$$

which has the numerical solution $\phi^*(\infty) \approx 0.615$. The numerical solution of eqs. (2.2a)–(2.2d) and (2.38a)–(2.38d) in the asymptotic limit, is displayed in Fig. 2.9 a). The threshold ratio of cells to patches $\phi^*(\infty)$ is robust with changes in k, varying weakly around 0.649. Because the curves $p_b(\phi)$ for each mechanism increase roughly the same with k, their intersection at $\phi^*(\infty)$ is robust. In Fig. 2.9 b), we see that $\phi^*(t)$ always begins at zero, but whether it monotonically increases or not depends on k. Allowing cell-cell adhesion may initially connect scaffolds faster, but suppressing it for $\phi \lesssim \phi^*$ will eventually result in larger scaffolds.

Bond probability p_b is maximized in the suppressed cell-cell adhesion case for $\phi = 0.5$, for which a significant gain is obtained when compared with allowing cell-cell adhesion. This gain increases as k decreases, as seen in Fig. 2.10. The mechanism that optimizes scaffold production is the one in which cell-cell adhesion is suppressed. This mechanism optimizes the density of particle-particle bonds, making for a larger scaffold that self-assembles faster. Henceforth, we will consider only the suppressed cell-cell adhesion model.

2.4 Percolation properties (mean-field)

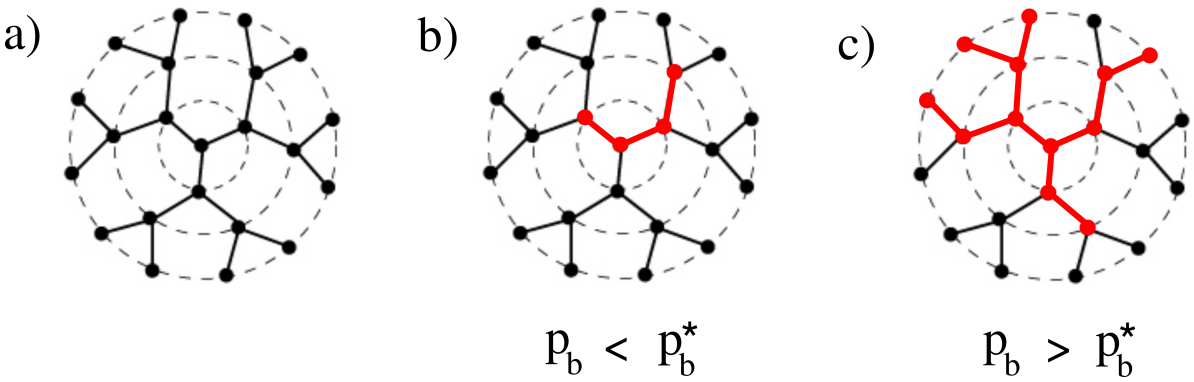

Figure 2.11: a) Bethe lattice for $f = 3$; c) and b) examples of aggregates that are and are not percolated, respectively. Red nodes and edges represent the aggregate. Image adapted from Cadilhe et al. (2007) [20].

Given the bond probability p_b obtained in section 2.1, it is possible to study the aggregation of the particles. We generalize to a case of particles with f patches. We neglect redundant bonds that link an aggregate to itself (loops). Aggregates are thus tree-like and cutting any bond causes the aggregate to split into two. Cell-mediated bonds are taken to be uncorrelated, every patch having the same probability

p_b of being linked to a patch of a different particle. Spatial correlations are neglected, a particle can form bonds to any other particle, so long as they do not exceed f bonds. Neglecting correlations corresponds to taking the limit of infinite spatial dimensions (mean-field percolation). The Bethe lattice, a graph in which all nodes have f neighbors and no loops are formed (see Fig 2.11 a)) is a lattice representation of such a geometry [21]. An aggregate can thus be represented as a subset of the Bethe lattice in which nodes are particles and edges are bonds (see Fig 2.11 b) and c)).

Depending on p_b, there will be two phases, one in which there is a gel, an aggregate that spans the entire system (in the thermodynamic limit, it is infinite); and one where no gel is present. The order parameter is the fraction of particles present in the gel $S(p_b)$, which is non-zero only when there is a gel. Gelation occurs at bond probabilities higher than a critical bond probability p_b^* [22]. On average, the number of bonds leading out of a particle is $(f-1)p_b$. In order to have an infinite system (see Fig 2.11 c)) , the number of bonds leading out of any particle must be larger or equal than one on average, where equality is the condition for the critical point [23],

$$p_b^* = \frac{1}{f-1}. \tag{2.49}$$

For $f = 6$ as in sections 2.1 and 2.2, the critical probability is $1/5$. Forming a scaffold requires gelation, as multiple disconnected aggregates do not provide the needed mechanical rigidity. In Fig. 2.12 a), we can see systems with $\phi < 0.1$ never form a scaffold. The interval of ϕ at which there is gelation has an upper-bound which is dependent on k, which means particles can be fabricated such that there is gelation even at high values of ϕ. Furthermore, it is possible to determine the time at which the gel is formed as function of ϕ, k_0 and k_1.

The existence of a gel does not require all particles of the system to belong to it. The fraction of particles in the giant aggregate S varies continuously from zero to one, and can provide information over the rheological and structural properties of the gel. As S increases, its surface area increases and the size of its pores decrease. Defining u as the probability that a random patch does not lead to the giant aggregate, the probability that a particle is not connected to the giant aggregate is u^f. As S is the probability that a particle is part of the giant aggregate,

$$S = 1 - u^f. \tag{2.50}$$

If a patch does not lead to the giant aggregate, either it forms no bond at all (with probability $1 - p_b$), or it leads to a particle that is also not part of the giant aggregate through other bonds (with probability $p_b u^{f-1}$). The sum of the two probabilities is the probability u.

$$u = 1 - p_b + p_b u^{f-1}, \tag{2.51}$$

uniquely determining the function $u(p_b)$ and, combined with eq. (2.50), determining the function $S(p_b)$. However, from eq. (2.51), it is not possible to obtain $u(p_b)$ analytically for a generic value of f, and we must resort to numerical methods, as in Fig. 2.12 b). The phase transition at $p_b = 1/5$ is clearly visible, corresponding to the critical values of $\phi = \{0.1, 0.9\}$ (in the limit $k \to 0$). $S(p_b)$ saturates quickly; increasing p_b above $1/2$ does not change the connectivity of the gel appreciably.

The rate eqs. (2.2a)–(2.2d), combined with eqs. (2.50) and (2.51), provide a theory that describes both the dynamics of the cells and of the scaffold as a whole. When developing it, we have always neglected correlations, which will lead to significant deviations from experiments on systems that are densely-packed, gelled, etc. In chapter 3, we introduce spatial correlations and study their effect through a lattice

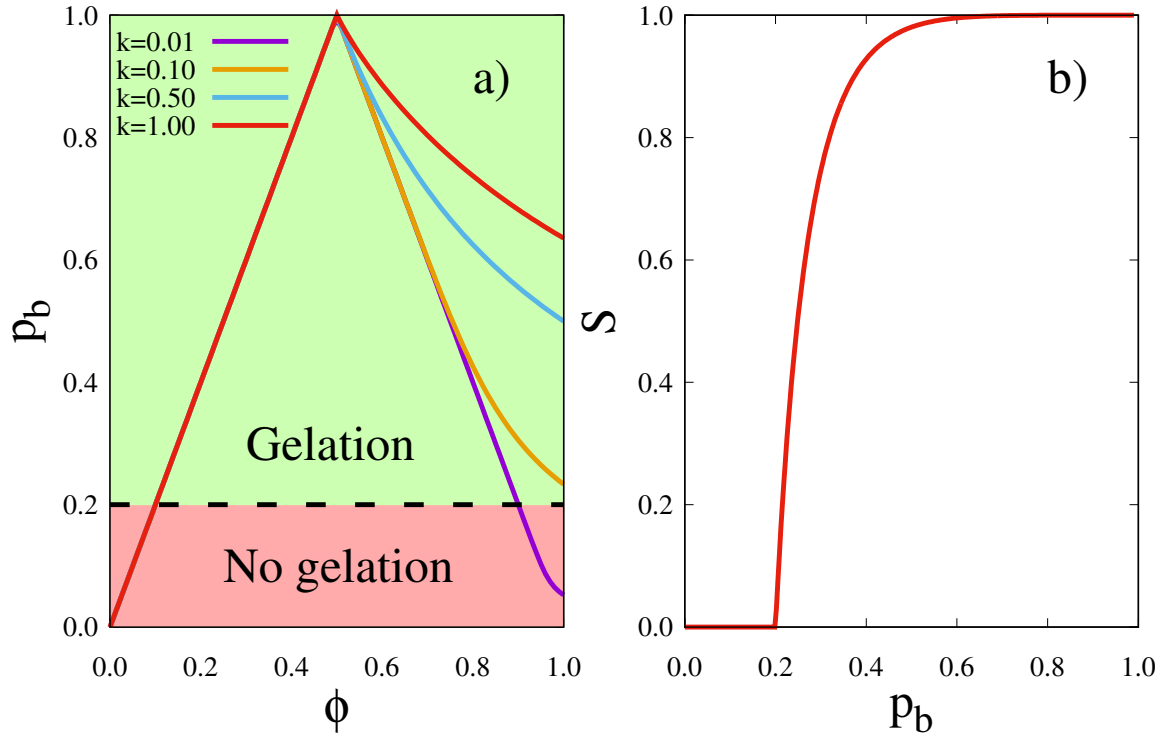

Figure 2.12: Percolation for $f = 6$. a) p_b as function of ϕ in the asymptotic limit. Values of p_b in the green region correspond to gels. b) Dependency of fraction of particles in giant aggregate on bond probability.

model.

Chapter 3

Lattice model

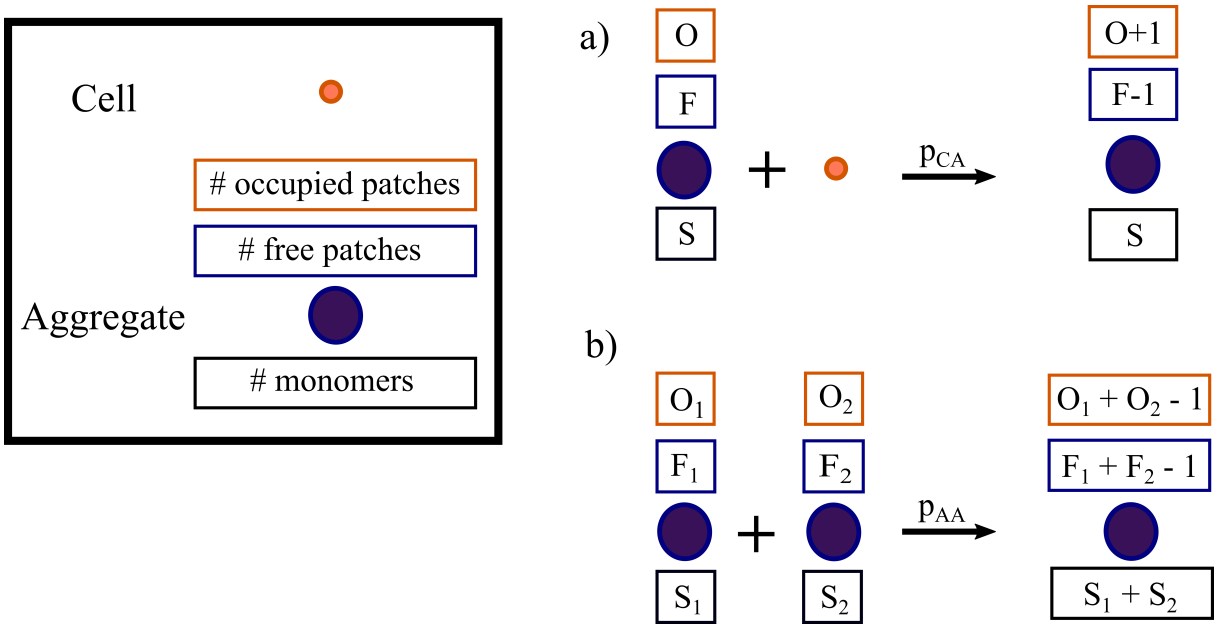

Figure 3.1: Illustration of the possible reactions of the lattice model: a) bond between a cell and an aggregate leads to a free patch becoming occupied; b) bond between two aggregates uses a free and occupied patch. All other patches remain accessible.

In chapter 2, we studied the dynamics of a 3D system of colloidal particles and cells through a mean-field set of rate equations. The mean-field approach neglects spatial correlations; to study their effect, we now discuss a lattice version of our model. Henceforth, particles are referred to as monomers. For simplicity, the term "aggregate" will include monomers. The size of an aggregate is defined as the number of monomers in it; free monomers are aggregates of size one.

Monomers occupy a lattice space and move by a sequence of random hops to their nearest neighbors. The hopping rate is related to the diffusion coefficient D_m. Monomers have f patches on their surface, which is the maximum number of bonds they can form. A patch can be free and form no bond or it can be occupied and form an irreversible bond to a cell. A patch cannot be occupied by more than one cell. A lattice space cannot be occupied by more than one monomer. The density of monomers n_m is defined as the ratio of lattice spaces occupied by monomers at $t = 0$. We study the very diluted regime ($n_m \ll 1$), and neglect the aggregate shape and orientation, as the characteristic time for aggregates to find each other is much larger than the timescale of rotational diffusion. We thus consider patches belonging to the same aggregate to be uncorrelated.

As in the previous chapter, there is a second species, the cells. Cells occupy a lattice space and hop with a rate related to their diffusion coefficient D_c. A lattice space can be occupied by at most one cell. The density of cells n_c is defined as the ratio of lattice spaces occupied by cells at $t = 0$. Cells form irreversible bonds to patches. By forming a bond to a maximum of two patches, they mediate bonds between monomers. When a cell attempts to hop to a lattice space occupied by an aggregate or vice versa, the cell forms a bond to the aggregate with a probability p_{CA} (see Fig. 3.1 a)),

$$p_{CA} = \frac{F}{F+O}, \tag{3.1}$$

where F and O are the number of free and occupied patches of the aggregate, respectively. p_{CA} is the the fraction of patches in the aggregate that are free.

When an aggregate attempts to hop to a space already occupied by another aggregate, they form a cell-mediated bond with probability p_{AA} (see Fig. 3.1 b)),

$$p_{AA} = \frac{F_1O_2 + O_1F_2}{(F_1+O_1)(F_2+O_2)}, \tag{3.2}$$

where $F_{1,2}$ and $O_{1,2}$ are the number of free and occupied patches and the subscript identifies the corresponding aggregate. p_{AA} is the fraction of pairs of patches, one from each aggregate, where one is free and the other is occupied. p_{AA} is zero when both aggregates only have free patches or only have occupied patches. Despite aggregates occupying one lattice space, aggregate characteristics such as size and number of occupied patches are taken into account through the probabilities p_{CA} and p_{AA}. If no bond is formed, the collision is elastic and the cell or aggregate that is moving returns to its initial position. No cell-mediated bonds may be formed between monomers belonging to the same aggregate.

The number of free patches F, occupied patches O, and size S of an aggregate are not independent. When two free monomers form a bond, the resulting dimer is such that $F = F_1 + F_2 - 1$ and $O = O_1 + O_2 - 1 = f - F_1 + f - F_2 - 1$. Generalizing for an aggregate composed of S monomers:

$$F = F_1 + F_2 - 1 + F_3 - 1 + \ ... = \sum_{i=1}^{S} F_i - (S-1), \tag{3.3}$$

$$O = f - F_1 + f - F_2 - 1 + f - F_3 - 1 + \ ... = Sf - \sum_{i=1}^{S} F_i - (S-1), \tag{3.4}$$

and thus,

$$F + O = S(f-2) + 2. \tag{3.5}$$

We measured the average size of the aggregates $\langle S \rangle(t)$ as a function of time defined as

$$\langle S \rangle = \frac{N}{N_{agg}}, \tag{3.6}$$

where N is the number of free monomers at $t = 0$ and $N_{agg}(t)$ is the number of aggregates as a function of time. As all monomers are free at $t = 0$, $N_{agg}(0) = N$. We have also measured the size $S_{max}(t)$ of the largest aggregate as a function of time, and the bond probability $p_b(t)$, defined as the probability that a patch forms a cell-mediated bond with a second patch as a function of time. Aggregates are tree-like and the number of bonds between the monomers composing an aggregate of size S is $S - 1$; as for every

bond, there are two patches,

$$p_b = \frac{2}{fN} \sum_{a=1}^{N_{agg}} (S_a - 1) = \frac{2(N - N_{agg})}{fN}, \tag{3.7}$$

where a indexes the aggregates and S_a is the size of the a-th aggregate. All monomers and cells start free. Let C be the number of cells at $t = 0$. We define ϕ as the ratio of cells to patches,

$$\phi = \frac{C}{Nf}. \tag{3.8}$$

An aggregate of size S will diffuse with the coefficient D_m^S. Since time can be rescaled, the dynamics does not depend on the absolute value of the diffusion coefficients, but on their relative value. We define Δ as the ratio of cell and free monomer diffusion coefficients:

$$\Delta = \frac{D_c}{D_m^1}. \tag{3.9}$$

Henceforth, we will rescale time such that $D_m^1 = 1$.
In section 3.1, we outline the algorithm used in the simulations; in section 3.2, we study the limit of all aggregates having the same diffusion coefficient; in section 3.3, we study the limit where only free monomers diffuse.

3.1 Computational methods

Simulations were performed on a 3D cubic lattice of linear length L_{box} with a Monte Carlo algorithm inspired on the kinetic Monte Carlo method [24,25], but with rejection sampling, as described below. As we study the limit $n_m \ll 1$, the discretization of the lattice does not significantly influence the results. Periodic boundary conditions were used. Cells hop with rate q_c and aggregates of size S hop with rate q_m^S. We keep track of the number of cells N_c and of aggregates of size S N_m^S. We consider hopping to be uncorrelated in space and time and so the total rate at which cells hop is $N_c q_c$, and the total rate at which aggregates of size S hop is $N_m^S q_m^S$. The total rate of hopping Q is then the sum over cells and aggregates of all sizes present in the simulation,

$$Q = N_c q_c + N_m^1 q_m^1 + N_m^2 q_m^2 + \ ... \ + N_m^{S_{max}} q_m^{S_{max}}. \tag{3.10}$$

A random uniform variable $\chi \in]0, 1]$ is generated and used to pick if a cell or a particle attempts to hop. The probability that a cell attempts to hop is $N_c q_c/Q$; the probability that an aggregate of size S attempts to hop is $N_m^S q_m^S/Q$. A second random uniform variable is generated to pick the specific aggregate or cell that hops. A third random uniform variable picks a direction in which the hop is attempted. The simulation clock is incremented whether the hop attempt is successful or not. As hopping is uncorrelated in time, the time between hops Δt is a random variable described by an exponential distribution and is generated by

$$\Delta t = -\frac{\log(\psi)}{Q}, \tag{3.11}$$

where ψ is a uniformly generated random variable. This method of incrementing the simulation clock preserves the correct time evolution, provided that we use the physical rates for each process.

To obtain the rates q_c and q_m^S, we discretize the diffusion equation [17]. For simplicity, we take the 1D case for a single monomer:

$$\frac{\partial m}{\partial t} = D_m^1 \frac{\partial^2 m}{\partial x^2}, \tag{3.12}$$

where $m(x,t)$ is the probability of finding the monomer in position x at time t, and D_m^1 is the diffusion coefficient of free monomers. Discretizing the partial derivatives in x, we obtain

$$\frac{\partial m}{\partial t} = D_m^1 \frac{m(x+\Delta x) + m(x-\Delta x) - 2m(x)}{\Delta x^2}, \tag{3.13}$$

where Δx is the lattice constant. An initial condition such that $m(x \pm \Delta x) = 0$ makes it clear that the hopping rate q_m^1 is $2D_m^1/\Delta x^2$. For 3D, we obtain

$$q_m^S = 6\frac{D_m^S}{\Delta x^2}. \tag{3.14}$$

In the simulations, we set $\Delta x = \sqrt{6}$ and rescaled time such that $q_m^1 = D_m^1 = 1$. All simulations were for $f = 6$.

To quantify the statistical error of a measurement, the standard error $\sigma_s(A)$ of measured quantity A was calculated,

$$\sigma_s(A) = \frac{\sigma(A)}{\sqrt{N_{samples}}}, \tag{3.15}$$

where $\sigma(A)$ is the approximated standard deviation of A calculated from the measurements, and $N_{samples}$ is the number of measurements.

3.2 Constant aggregate diffusion coefficient

We study the limit where all aggregates diffuse with the same coefficient,

$$D_m^S = D_m^1 = 1. \tag{3.16}$$

In eqs. (2.2a)–(2.2d), k is the ratio between the rate of cells forming a second bond and the rate of cells forming a first bond. When $k \ll 0$, all cells form one bond before any cell can form two. If $\phi \approx 0$, the density of occupied patches after all cells form one bond will be much lower than the density of free patches. Conversely, if $\phi \approx 1$, the density of free patches after all cells form one bond will be much lower than the density of occupied patches. As both occupied and free patches are required to form a bond, and because low densities decrease the effect of spatial correlations, the mean-field rate equations fit the simulations better for $\phi \approx \{0, 1\}$. Figure 3.2 shows spatial correlations between aggregates have a significant effect on the dynamics, as the number of cells with zero, one and two bonds (C_0, C_1, C_2, respectively) obtained from eqs. (2.2a)–(2.2d) and from the simulations deviate significantly outside of the limits $\phi \approx \{0, 1\}$. Note that C_0 in the lattice model corresponds to the number of free cells, C_1 to the sum of all occupied patches, and C_2 can be inferred from the number of aggregates N_{agg} as in eq. (3.7). Figure 3.3 shows that $\langle S \rangle$, S_{max}, and p_b are non-monotonic as a function of ϕ and exhibit a constant value for $\phi \in [1/6, 5/6]$ in the asymptotic limit. To understand these results, we start by assuming an interval of ϕ exists for which all cells form cell-mediated bonds and calculate the asymptotic value of

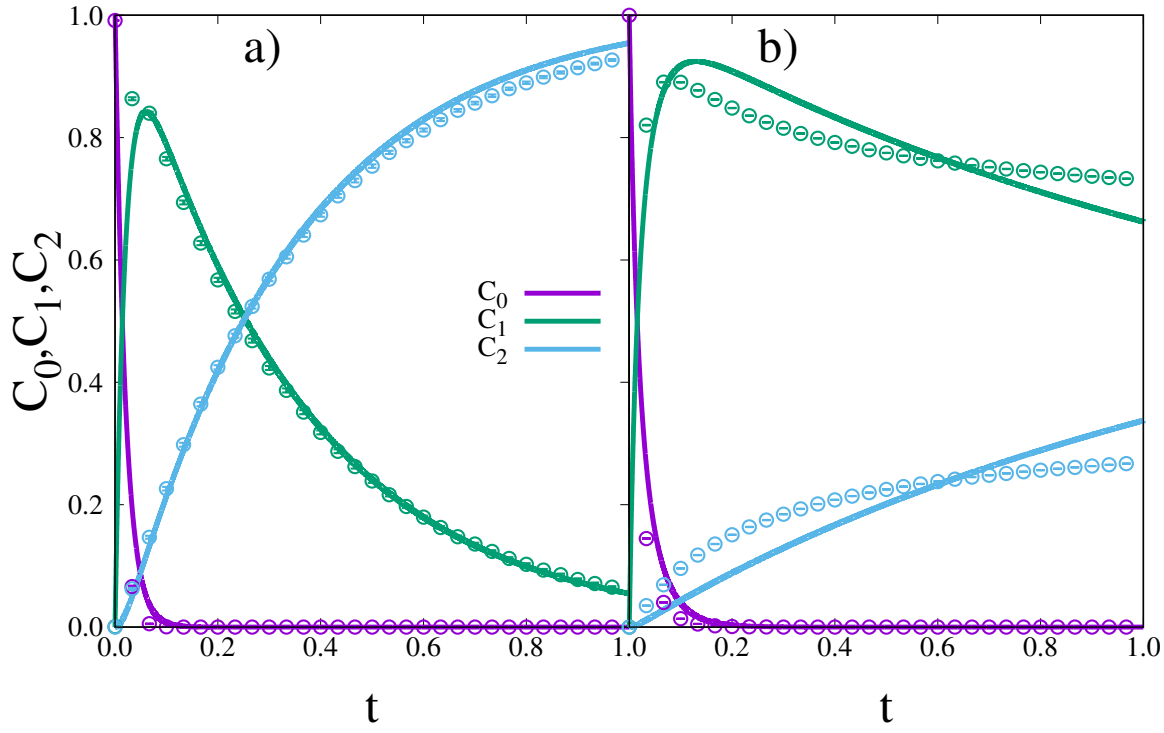

Figure 3.2: Comparison between the time evolution of the concentration of different types of cells as given by eqs. (2.2a)–(2.2d) (lines) and from simulations (points) for $f = 6$, $n_m = 0.1$, $\Delta = 10$ and $\phi = \{0.01, 0.5\}$ for a) and b) respectively. C_0 is the number of cells with zero bonds, C_1 is the number of cells with one bond, and C_2 is the number of cells with two bonds. Results normalized such that $C_0 + C_1 + C_2 = 1$. Lines were obtained by fitting parameters k_0 and k_1 through the minimum squares method, resulting in $k \approx \{0.06, 0.02\}$. Results averaged over 200 samples.

$\langle S \rangle$ in that interval. As aggregates are tree-like, for every cell-mediated bond, two aggregates merge:

$$N_{agg}(\infty) = N - C = \frac{C}{f\phi} - C. \tag{3.17}$$

Using eqs. (3.6) and (3.17), we find $\langle S \rangle$ for the interval of ϕ for which all cells form two bonds eventually.

$$\langle S \rangle(\infty) = \frac{N}{N - C} = \frac{1}{1 - f\phi}\ ,\ \phi \leq \frac{1}{f}. \tag{3.18}$$

In eq. (3.18), $\langle S \rangle$ diverges at $\phi = 1/f$, which corresponds to one cell per monomer; in this case, all monomers will eventually belong to the same aggregate (see Fig. 3.4 b)) and $\langle S \rangle = S_{max} = N$. A larger value of ϕ does not result in more cell-mediated bonds because aggregates are tree-like and there cannot be more bonds than $N - 1$. If there is more than $f - 1$ cells per monomer, not all monomers can form cell-mediated bonds due to lack of empty patches. There arises a competition between cells with one bond and free cells for the last empty patches. $\langle S \rangle$ is thus determined by Δ. In the limit of cells diffusing must faster than aggregates ($\Delta \to \infty$), dynamics are split in two regimes. The first is the cell regime, in which only cells diffuse. All cells form one bond in the cell regime for $\phi \leq 1$. When $\Delta \to \infty$ and $\phi = 1$, all patches are occupied at the end of the cell regime, thus a larger number of cells such that $\phi > 1$ does not influence the aggregation. The interesting range when $\Delta \to \infty$ is $\phi \in [0, 1]$. Afterwards comes the aggregate regime, in which only aggregates diffuse. For $\phi > (f - 1)/f$, all free patches form

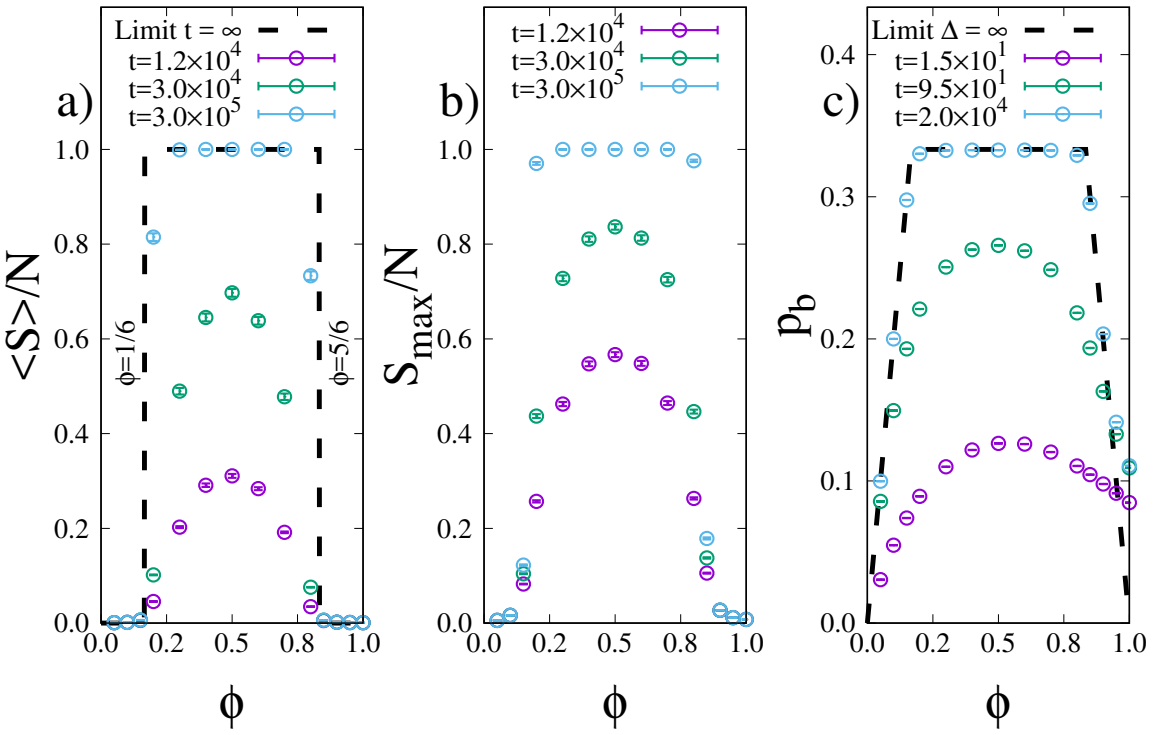

Figure 3.3: Aggregate measurements as a function of ϕ for different values of time: a) normalized average size of the aggregates $\langle S\rangle/N$, where the dashed line is the result of eqs. (3.21a) and (3.21b); b) normalized size of the largest aggregate S_{max}/N; c) bond probability p_b, where the dashed line curve is the result of eqs. (3.22a)–(3.22c). Parameters are $L_{box} = 25$, $f = 6$, $n_m = 0.1$, $\Delta = 10$. Simulations were averaged over 1000 samples.

cell-mediated bonds in the aggregate regime and,

$$N_{agg}(\infty) = N - (Nf - C) = \frac{C}{f\phi} - \left(\frac{C}{\phi} - C\right). \tag{3.19}$$

From eqs. (3.6) and (3.19) follows,

$$\langle S\rangle(\infty) = \frac{N}{N - (Nf - C)} = \frac{1}{1 + f(\phi - 1)}, \frac{f-1}{f} < \phi \leq 1. \tag{3.20}$$

Combining eqs. (3.18) and (3.20), and dividing by N, we obtain the asymptotic normalized average size of the aggregates. Taking the thermodynamic limit ($N \to \infty$), we obtain

$$\lim_{N\to\infty} \frac{\langle S\rangle}{N}(\infty) = \begin{cases} 1 & , \frac{1}{f} \leq \phi \leq \frac{f-1}{f}, \quad (3.21a) \\ 0 & , \text{otherwise.} \quad (3.21b) \end{cases}$$

For $f = 6$, we obtain discontinuities in $\phi = \{1/6, 5/6\}$, which is in agreement with the simulations. With calculations similar to eqs. (3.18) and (3.20), we obtain,

$$p_b(\infty) = \begin{cases} 2\phi, & \phi \leq \frac{1}{f}, \quad (3.22a) \\ \frac{2}{f}\left(1 - \frac{1}{N}\right) & \frac{1}{f} \leq \phi \leq \frac{f-1}{f}, \quad (3.22b) \\ 2 - 2\phi, & \frac{f-1}{f} \leq \phi \leq 1. \quad (3.22c) \end{cases}$$

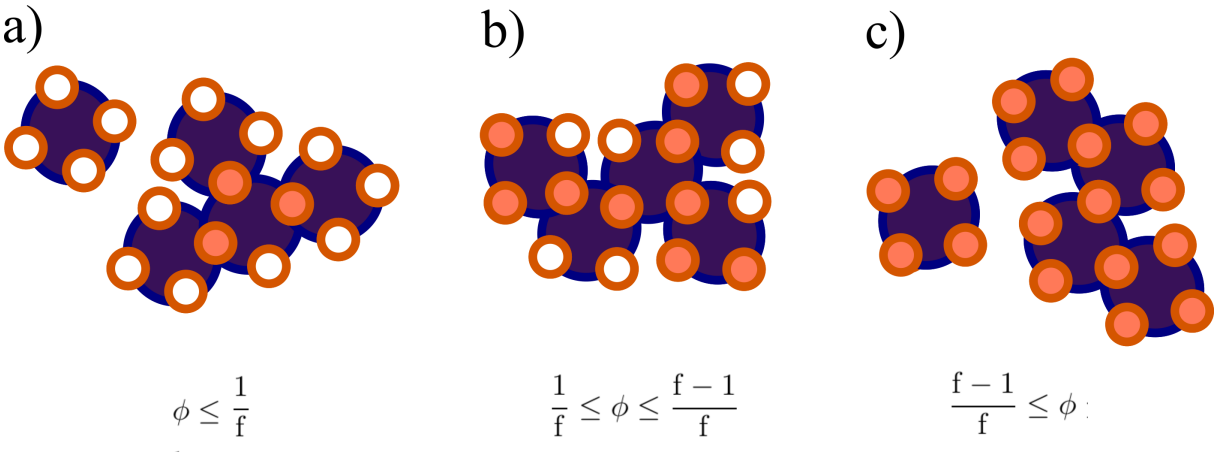

Figure 3.4: Illustration of the three ways dynamics cease. Monomers in purple. Hollow orange circles represent empty patches and filled orange circles represent occupied patches. a) When there is less than one cell per monomer, dynamics cease due to a lack of cells; b) when there is between one and $f-1$ cell per monomer, dynamics cease due to all monomers forming one aggregate; c) when there is more than $f-1$ cells per monomer, dynamics cease due to a lack of free patches.

Figure 3.3 shows $\langle S \rangle$, S_{max}, and p_b are maximized for $\phi = 0.5$ for finite times. This is expected as it corresponds to an equal number of occupied and free patches. However, p_b takes values comparable with the asymptotic state much faster than $\langle S \rangle$. From eqs. (3.6) and (3.7), we obtain

$$\frac{\langle S \rangle}{p_b} = \frac{f}{2} \frac{\langle S \rangle^2}{\langle S \rangle - 1}. \tag{3.23}$$

Deriving both sides of eq. (3.7) results in,

$$\dot{p}_b \langle \dot{S} \rangle^{-1} = \frac{2}{f \langle S \rangle^2}. \tag{3.24}$$

Combining eqs. (3.23) and (3.24), we obtain

$$\frac{\dot{p}_b}{p_b} \left(\frac{\langle \dot{S} \rangle}{\langle S \rangle} \right)^{-1} = \frac{1}{\langle S \rangle - 1}. \tag{3.25}$$

At initial times, when $\langle S \rangle \approx 1$, the ratio of the relative variation in p_b is much larger than the relative variation of $\langle S \rangle$. At later times, when $\langle S \rangle \gg 1$, the opposite happens. Thus p_b is not a good variable if one is interested in the time evolution of large tree-like aggregates.

When Δ is finite and the timescales of aggregate and cell diffusion are not separable, cell-mediated bonds can occur between aggregates before all cells form a bond. For $\phi < \frac{1}{f}$, the asymptotic value of $\langle S \rangle / N$, S_{max}/N and p_b does not depend on Δ. It does not matter if all cells form a bond before aggregates form cell-mediated bonds as there are enough free patches for all cells to form two bonds eventually. For tree-like aggregates, the number of cell-mediated bonds cannot be larger than $N-1$. For $\frac{1}{f} < \phi < \frac{f-1}{f}$, there is between one and $f-1$ cells per monomer and all monomers eventually form cell-mediated bonds, regardless of the value of Δ.

When $\Delta \to \infty$ and $\phi > \frac{f-1}{f}$, there are less empty patches than there are monomers at the end of the cell regime and a giant aggregate that contains all monomers cannot form. When Δ is finite, there arises a competition for the last free patches between free cells and cells with one bond, which is regulated by

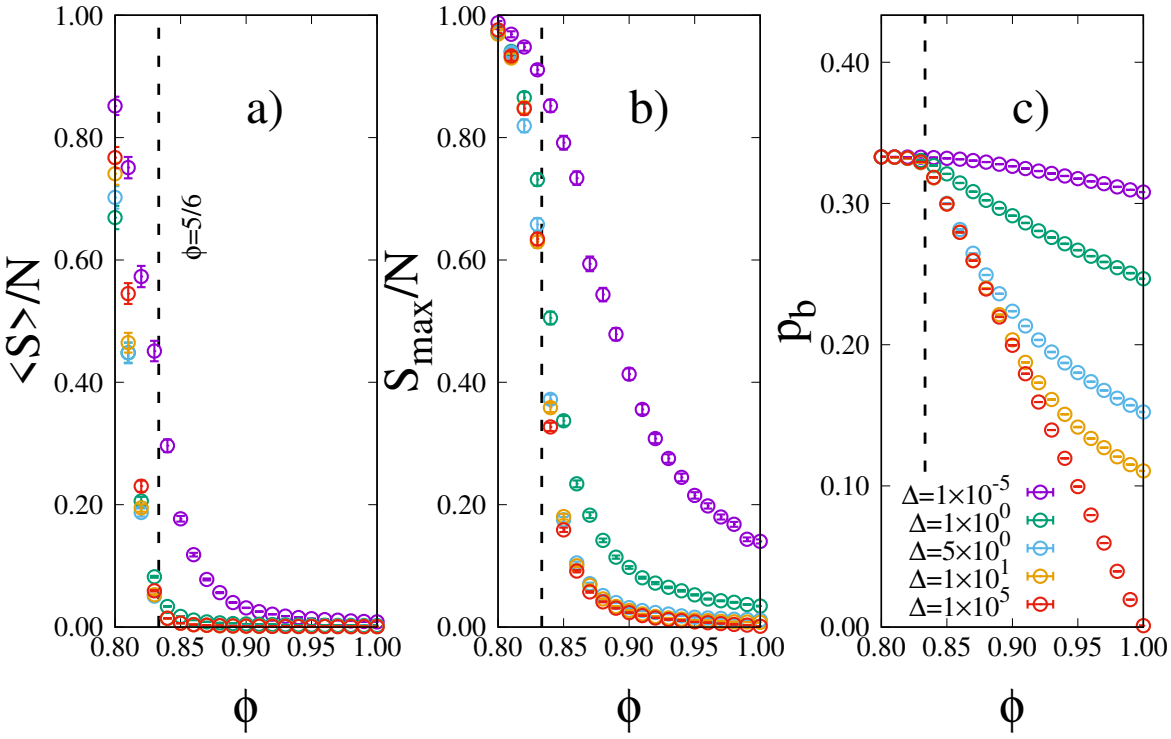

Figure 3.5: Aggregate measurements as a function of ϕ for different values of Δ at $t = 3 \times 10^5$: a) normalized average size of the aggregates $\langle S \rangle / N$; b) normalized size of the largest aggregate S_{max}/N; c) bond probability p_b. Parameters are $L_{box} = 25$, $f = 6$, $n_m = 0.1$, $D_m = 1$. Simulations were averaged over 250 samples. The dashed line corresponds to $\phi = 5/6$, which is predicted to be the lower bound of the interval of ϕ in which the asymptotic values of $\langle S \rangle$, S_{max} and p_b depend on Δ.

Δ. The faster aggregates diffuse when compared to cells, the likelier it is to find other aggregates and form a cell-mediated bond before free cells can form bonds to the remaining empty patches; thus a lower value of Δ results in increased $\langle S \rangle / N$, S_{max}/N, and p_b.

Figure 3.5 shows $\langle S \rangle / N$, S_{max}/N, and p_b at $t = 3 \times 10^5$ for three values of Δ for which the timescales of cell and aggregate diffusion are not separable, as well as the limits $\Delta \gg 1$ and $\Delta \ll 1$. It was found that increasing Δ above 10^5 or decreasing Δ below 10^{-5} did not change the three measurements at the simulated density of $n_m = 0.1$. Unphysical effects regarding the discretization of the lattice arise at higher values of n_m. Because the lattice model of this chapter is most valid in the limit $n_m \to 0$, a study of the influence of n_m is not provided in this chapter. Chapter 4 goes into greater detail on the effects of n_m and of finite-size effects.

To obtain a more complete picture of the dynamics, we introduce the weighted size distribution $d(S,t)$, defined as the fraction of monomers which are part of aggregates of size S at time t. Note that $d(S = 1, t)$ is the number of free monomers and

$$\sum_{S=1}^{\infty} d(S,t) = 1. \tag{3.26}$$

$d(S,t)$ is related to the standard size distribution $s(S,t)$, defined as the fraction of aggregates which have size S at time t through

$$d(S,t) = \frac{s(S,t)S}{\sum_{l=1}^{\infty} s(l,t)l} = \frac{1}{\langle S \rangle(t)}\, s(S,t)S. \tag{3.27}$$

In the thermodynamic limit, $d(S,t)$ is the probability that a randomly picked monomer is part of an aggregate of size S at time t, describing the importance of each size to the dynamics more directly than

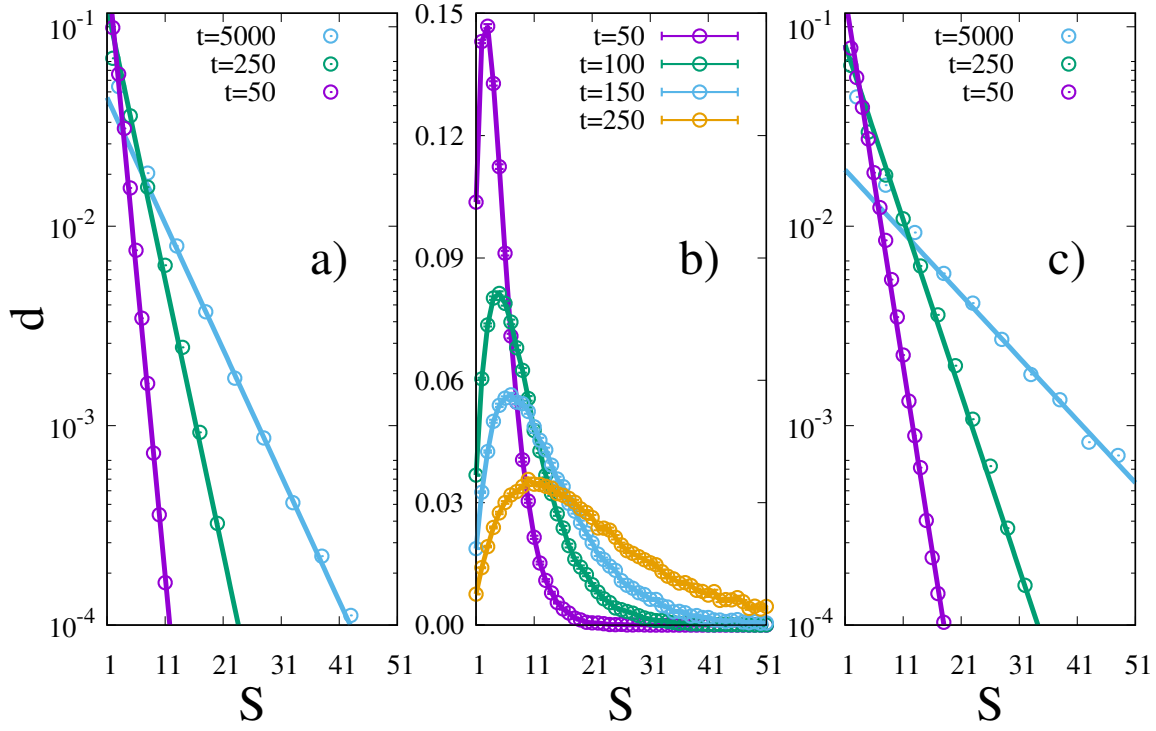

Figure 3.6: Size distribution d for different values of time, representing the fraction of monomers which are part of aggregates of size S. Ratio of cells to patches $\phi = \{0.1, 0.5, 0.9\}$, corresponding to a), b) and c), respectively. Points are simulation data with parameters $L_{box} = 25$, $f = 6$, $n_m = 0.1$, $\Delta = 10$; lines are linear fits. Results were averaged over 500 samples. In b) and c), the green and blue points have been binned. Green points are the average of three points; blue points are the average of five points.

$s(S, t)$.

Figures 3.6 a) and c) show distributions with an exponential tail, which is also present for $\phi = \{0.05, 0.16, 0.84, 0.95\}$, with only the rate parameter changing (results not shown). We conclude that

$$d(S,t) \sim e^{\lambda(t)S}, \quad \phi \leq \frac{1}{f} \vee \phi \geq \frac{f-1}{f}, \tag{3.28}$$

$$s(S,t) \sim \frac{e^{\lambda(t)S}}{S}, \quad \phi \leq \frac{1}{f} \vee \phi \geq \frac{f-1}{f}, \tag{3.29}$$

where $\lambda(t)$ is a function of time that changes with ϕ. For $\frac{1}{f} \leq \phi \leq \frac{f-1}{f}$ and for initial times, Fig. 3.6 b) shows that $d(S,t)$ flattens, meaning the probability of finding a monomer in an aggregate of size S is not dominated by a specific value of S. Not shown is the limit $d(S, t \to \infty) = \delta_{S,N}$ ($\delta_{i,j}$ is the Kroenecker delta), where all monomers form a single aggregate.

3.3 Diffusion of only free monomers

In this section, we study the limit where diffusion of aggregates with size larger than one can be neglected in the timescale of free monomer diffusion. For simplicity, hereafter we will refer to these aggregates as simply "aggregates". There are thus three timescales in the limit $\Delta \to \infty$, and the dynamics separate into three regimes. First is the cell regime, in the diffusion of cells dominates. All cells form one bond in the cell regime. Afterwards is the monomer regime in which the diffusion of free monomers dominates. Finally there is the aggregate regime where the diffusion of aggregates dominates. We study only the

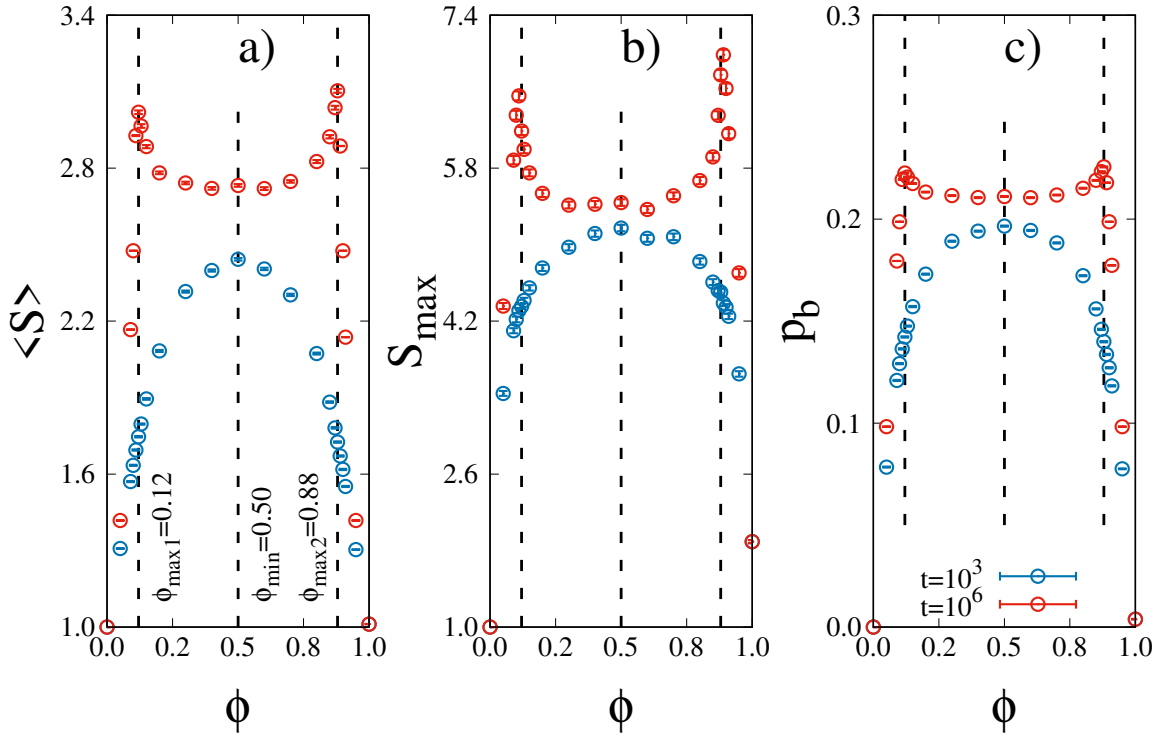

Figure 3.7: Aggregate measurements as a function of ϕ for different values of time: a) average size of the aggregates $\langle S \rangle$; b) size of the largest aggregate S_{max}; c) bond probability p_b. Parameters are $L_{box} = 25$, $f = 6$, $n_m = 0.01$, $\Delta = 1000$. Simulations were averaged over 500 samples.

first two regimes and set

$$D_p^S = D_p^1 \delta_{S,1} = \delta_{S,1}. \tag{3.30}$$

Figure 3.7 shows that $\langle S \rangle$ is initially maximized at $\phi = 0.5$ as seen in section 3.2, however the asymptotic state is fundamentally different from the ones seen before, as all three quantities exhibit a bimodal shape with local maxima in $\phi = \{0.12, 0.88\} \pm 0.01$ and $\phi = 0.5 \pm 0.1$ corresponding to a local minimum.

Let us consider the distribution of occupied patches per monomer $d_O(n)$, defined as the probability that a monomer has n occupied patches immediately after the cell regime. Immediately after the cell regime, all monomers are free. To obtain $d_O(n)$, we solve a set of mean-field rate equations for the cell regime as in chapter 2. Assuming that the rate of cells forming a bond with a monomer per unit time is proportional to its number of free patches,

$$\dot{C}_0 = -q\, C_0 \sum_{i=0}^{f} (f-i) M_i, \tag{3.31a}$$

$$\dot{M}_0 = -q\, C_0\, f M_0, \tag{3.31b}$$

$$\dot{M}_i = q\, C_0 \Big\{ \big[(f-(i-1)\big] M_{i-1} - (f-i) M_i \Big\},\ 1 \leq i \leq f, \tag{3.31c}$$

where $C_0(t)$ is the number of free cells as a function of time, $M_i(t)$ is the number of monomers with i occupied patches, and q is a rate constant that sets the timescale and does not influence the asymptotic

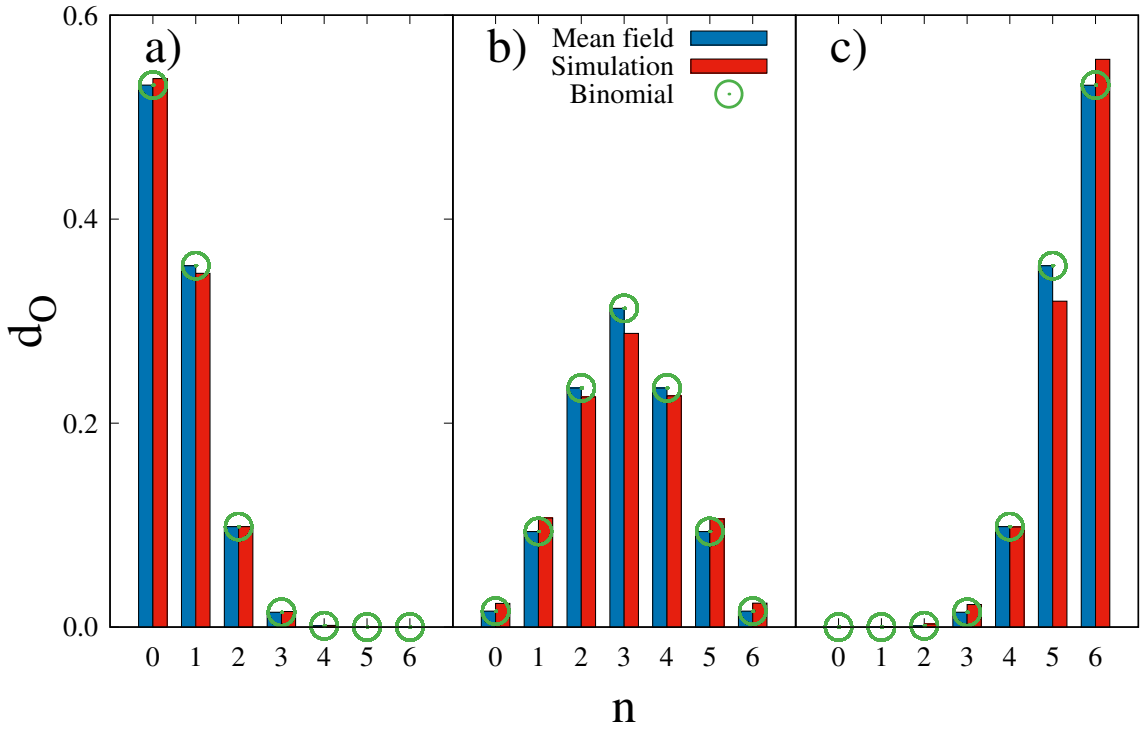

Figure 3.8: Occupied patch distribution for $\phi = \{0.1, 0.5, 0.9\}$ corresponding to a), b), and c), respectively). Parameters are $L_{box} = 25$, $f = 6$, $n_m = 0.01$, $\Delta = \infty$. Simulations were averaged over 500 samples. $\Delta = \infty$ was simulated by rejecting every monomer hop until all cells formed a bond.

result. The initial conditions for eqs. (3.31a)–(3.31c) are

$$C_0(0) = \phi f N, \tag{3.32a}$$

$$M_i(0) = N\delta_{i,0} \ , \ 0 \leq i \leq f, \tag{3.32b}$$

where N is the total number of free monomers which is conserved in the cell regime. Thus,

$$d_O(n) = \frac{M_n(\infty)}{N}. \tag{3.33}$$

As can be seen in Fig. 3.8, the asymptotic solution of eqs. (3.31a)–(3.31c) is a binomial distribution with f trials and probability of success equal to the ratio of cells to patches ϕ,

$$d_O(n) = \binom{f}{n} \phi^n (1-\phi)^{f-n}, \tag{3.34}$$

and is in agreement with simulations.

If there is much less than one linker per monomer, monomers with only free patches dominate; if there is between one and $f-1$ cells per monomer, monomers with both free and occupied patches dominate; if there is much more than $f-1$ linkers per monomer, monomers with only occupied patches dominate. Since it requires one free and one occupied patch to form a bond, free monomers with both occupied and free patches can form bonds with any other free monomer. By contrast, free monomers with only occupied patches cannot form bonds among each other, likewise for free monomers with only free patches. As aggregates are immobile, they may only grow through linker-mediated bonds with free monomers. If there is much less than one cell per monomer, all cells form a second bond but they are not numerous

enough for all monomers to form cell-mediated bonds in the asymptotic limit. Larger values of ϕ result in a larger number of cells and $\langle S \rangle$. Figure 3.9 a) shows that the values of $\phi = \{0.12, 0.88\} \pm 0.01$

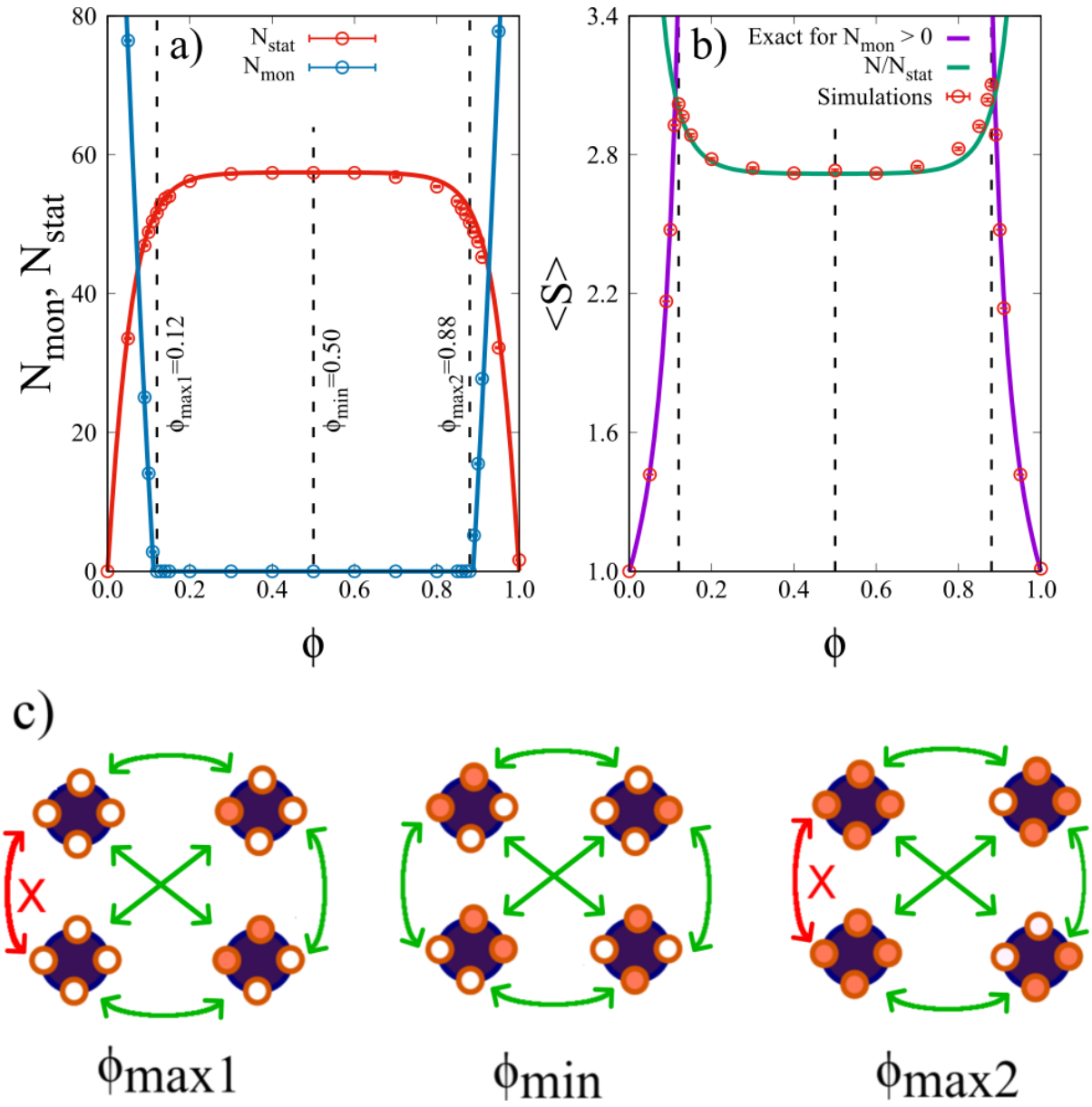

Figure 3.9: a) Asymptotic number of free monomers N_{mon} and number of aggregates of size larger than one N_{stat}; b) average size of the aggregates $\langle S \rangle$. Points are simulation data with parameters $L_{box} = 25$, $f = 6$, $n_m = 0.01$, $\Delta = 10^3$. Results were averaged over 500 samples. Purple lines in b) are obtained from eqs. (3.18) and (3.20). Green line in b) and both lines in a) are obtained from the asymptotic numerical solution of eqs. (3.35a)–(3.35c); the blue line in a) also requires the use of eq. (3.38); c) diagram illustrating the mechanism behind the maxima; particles in purple, empty orange circles are free patches and filled orange circles are occupied patches. Monomers with only free or occupied patches must form bonds to monomers with both free and occupied patches. When monomers with both free and occupied patches dominate, the tendency is to mainly form dimers.

corresponding to the maxima coincide with the edges of the interval of ϕ in which all monomers form cell-mediated bonds in the asymptotic limit (number of free monomers $N_{mon} = 0$). In this limit and interval, $\langle S \rangle$ is determined by the number of aggregates. Monomers with only free or occupied patches cannot form cell-mediated bonds with each other. A distribution $d_O(n)$ with less of these monomers increases the number of aggregates (mostly as dimers) and decreases $\langle S \rangle$. Figure 3.9 a) shows the number of aggregates is maximized at $\phi = 0.5$, which corresponds to the value of ϕ that maximizes $\sum_{n=1}^{f-1} d_O(n)$.

The values of ϕ which minimize the number of monomers with both free and occupied patches in the interval in which $N_{mon} = 0$ thus correspond to the maxima in $\langle S \rangle$. The smaller of those values is $\phi = 0.12 \pm 0.01$. If there is much more than $f - 1$ cells per monomer, the number of free patches after the cell regime is not enough for all monomers to form cell-mediated bonds. Larger values of ϕ decrease the number of free patches and $\langle S \rangle$. The mechanism behind the first maximum leads to a second maximum in $\langle S \rangle$ at $\phi = 0.88 \pm 0.01$. When $\Delta \to \infty$ and spatial correlations can be neglected, the dynamics are symmetrical to swapping free and occupied patches and $\langle S \rangle$ is symmetrical with respect to $\phi = 0.5$.

We calculate the number of aggregates N_{stat} with a set of mean-field balance equations for the monomer regime using the distribution d_O as initial conditions. Following the same principles as in chapter 2, we define $N_{stat}(t)$ as the number of aggregates as a function of time, $N_{both}(t)$ as the number of free monomers with both free and occupied patches, and $N_{only}(t)$ as the number of free monomers with only free or occupied patches,

$$\dot{N}_{stat} = q_0 \, N_{both} N_{only} + \frac{q_0}{2} \, N_{both}^2, \tag{3.35a}$$

$$\dot{N}_{both} = -q_0 \, N_{both} N_{only} - q_0 \, N_{both}^2 - q_1 \, N_{both} N_{stat}, \tag{3.35b}$$

$$\dot{N}_{only} = -q_0 \, N_{both} N_{only} - q_1 \, N_{only} N_{stat}, \tag{3.35c}$$

with initial conditions,

$$N_{stat}(0) = 0, \tag{3.36a}$$

$$N_{both}(0) = N \sum_{n=1}^{f-1} d_O(n), \tag{3.36b}$$

$$N_{only}(0) = N(\, d_O(0) + d_O(f) \,), \tag{3.36c}$$

where N is the number of monomers at $t = 0$. In eqs. (3.35a)–(3.35c), we have neglected aggregates with only free or occupied patches by performing the approximation that all free monomers can form bonds to all aggregates. We neglected also the effect of the size of aggregates and of the number of free and occupied patches of free monomers and aggregates on the aggregation rates by considering constant rate constants q_0 and q_1. Free monomers form bonds with each other at a rate q_0 and with aggregates at a rate q_1. Since aggregates are immobile, $q_1 = q_0/2$ [18]. The absolute value of q_0 does not influence the asymptotic result. We have also neglected aggregation between monomers with only occupied patches and only free patches. The shape of eq. (3.34) is such that aggregation between these two monomers is much rarer than aggregation between them and monomers with both free and occupied patches for all values of ϕ.

Figure 3.9 b) shows N/N_{stat} obtained from the asymptotic numerical solutions of eqs. (3.35a)–(3.35c). For $\phi \in [0.12, 0.88]$, the asymptotic number of free monomers is zero and $N/N_{stat} = \langle S \rangle$. When the asymptotic number of free monomers is different from zero, we may use eqs. (3.18) and (3.20) to obtain $\langle S \rangle$. The values of ϕ which correspond to the maxima in $\langle S \rangle$ can be obtained by the intersections of $\langle S \rangle$ obtained from eqs. (3.18) and (3.20) with N/N_{stat} obtained from eqs. (3.35a)–(3.35c). These intersections coincide with the edges of the interval of ϕ in which $N_{mon} = 0$ and thus with the maxima in $\langle S \rangle$. The maxima derived theoretically are in very good agreement with the ones obtained from the simulations, as shown in Fig. 3.9 b), validating our proposed mechanism.

We define the average size of aggregates $\langle S \rangle_{stat}$

$$\langle S \rangle_{stat} = \frac{N - N_{mon}}{N_{stat}}, \tag{3.37}$$

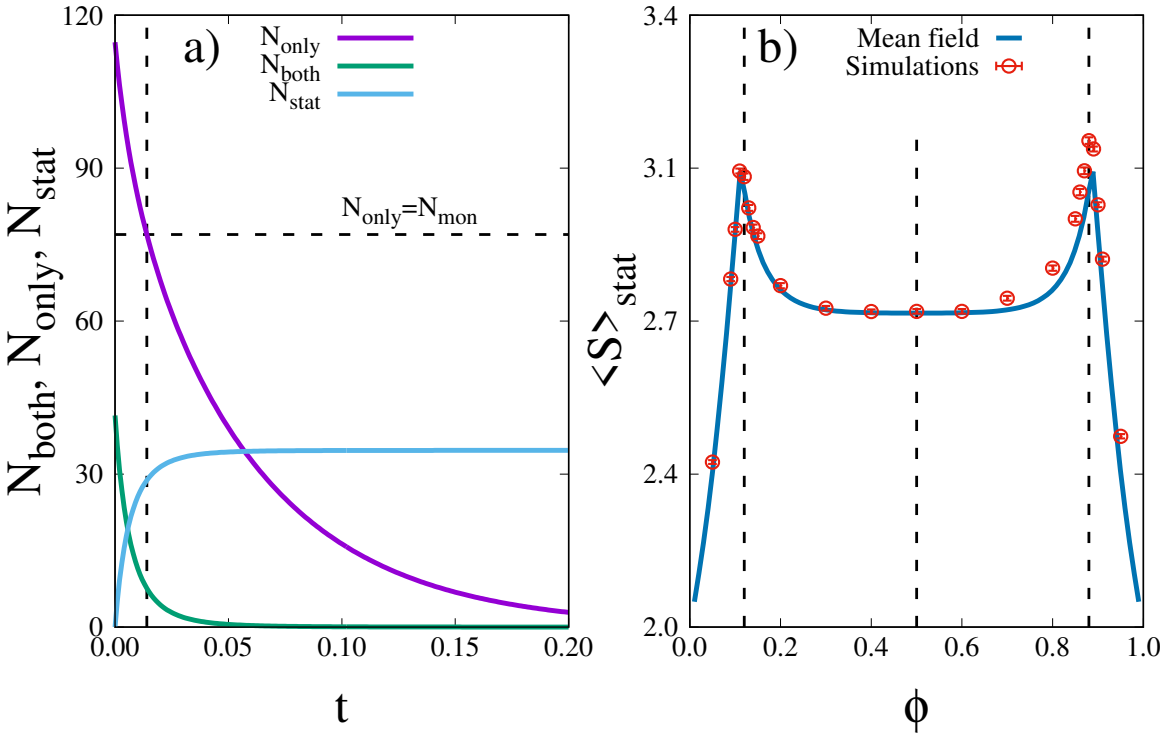

Figure 3.10: a) Numerical solution of eqs. (3.35a)–(3.35c) for the number of free monomers with only free or occupied patches N_{only}, number of free monomers with both free and occupied patches N_{both}, and number of aggregates of size larger than one N_{stat} as functions of time. Parameters are $\phi = 0.05$ and $q_0 = 1$. Dashed lines mark the point in which N_{only} is equal to N_{mon} calculated from eq. (3.38) using the asymptotic N_{stat} as well as eqs. (3.18) and (3.20); b) average size of the aggregates of size larger than one $\langle S\rangle_{stat}$. Points are simulation data with parameters $L_{box} = 25$, $f = 6$, $n_m = 0.01$, $\Delta = 10^3$. Results were averaged over 500 samples. Lines were obtained using eqs. (3.18), (3.20), (3.35a)–(3.35c), and (3.38).

where $N - N_{mon}$ is the number of monomers that are part of aggregates. Figure 3.10 b) shows $\langle S\rangle_{stat}$ exhibits a bimodal shape with its maxima in the same values of ϕ as $\langle S\rangle$. The mechanism is similar as for $\langle S\rangle$. When there is much less than one cell per monomer, monomers with zero or one occupied patches dominate; only dimers can form and $\langle S\rangle_{stat} = 2$. A larger number of cells enables the formation of larger aggregates until there are enough cells for all monomers to form a cell-mediated bond; $\langle S\rangle_{stat} = \langle S\rangle$ for $\phi \in [0.12, 0.88]$. If there is much more than $f - 1$ cells per monomer, monomers with $f - 1$ and f occupied patches dominate and only dimers can form.

Knowing that the total number of aggregates of all sizes $N_{agg} = N_{mon} + N_{stat}$, we rearrange equation (3.6),

$$N_{mon} = \frac{N}{\langle S\rangle} - N_{stat}. \tag{3.38}$$

N_{stat} is obtained from eqs. (3.35a)–(3.35c). Meanwhile, when $N_{mon} \neq 0$ in the asymptotic limit, $\langle S\rangle$ is obtained from eqs. (3.18) and (3.20). We can therefore calculate N_{mon} using eq. (3.38) and $\langle S\rangle_{stat}$ (see Fig. 3.9 a) and b)).

Equations (3.35a)–(3.35c) predict all monomers form bonds with aggregates for all values of ϕ (asymptotically $N_{both}, N_{only} \to 0$), which is seemingly incompatible with the results of Fig. 3.9 a)). To understand why the calculated values of N_{mon}, N_{stat}, $\langle S\rangle$, and $\langle S\rangle_{stat}$ match the simulations despite this difficulty, we show in Fig. 3.10 a) the time evolution of N_{both} and N_{only} for a value of ϕ in which $N_{mon} \neq 0$. Because N_{both} tends to zero earlier than N_{only} and because N_{only} cannot form aggregates with itself, after some time N_{stat} remains approximately constant despite the value of N_{only}. We then calculate the correct value of N_{mon} using eqs. (3.18), (3.20), and (3.38).

Chapter 4

The role of the shape of aggregates

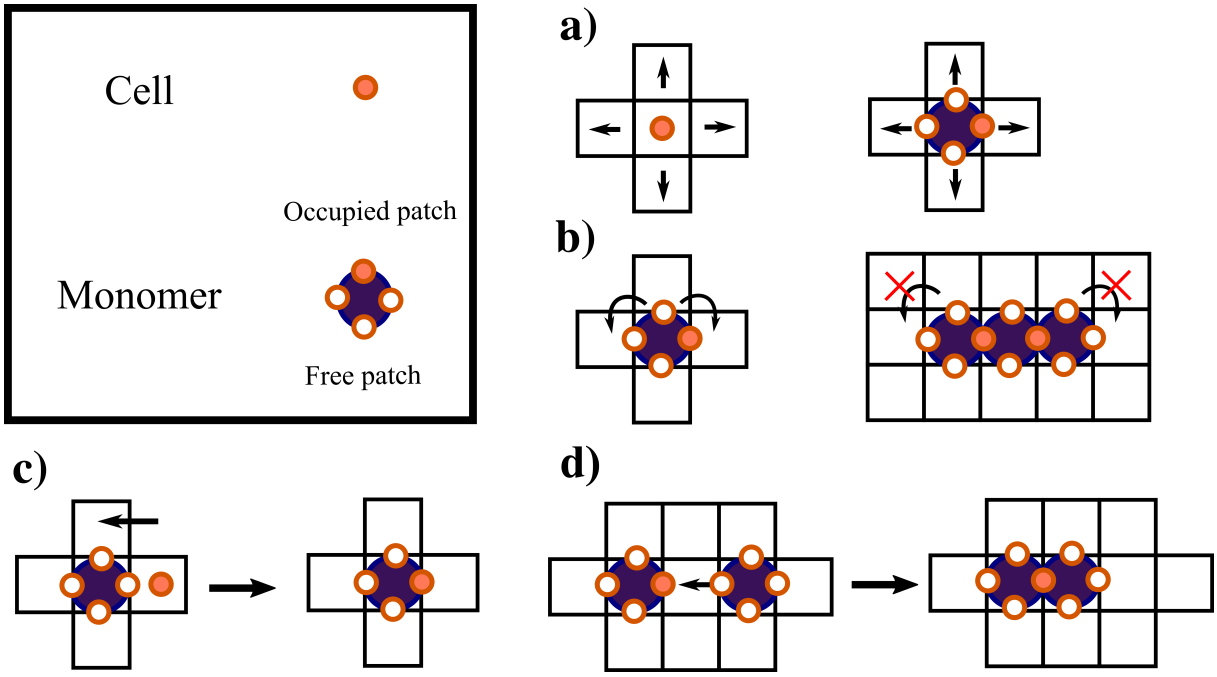

Figure 4.1: Illustration of the main ingredients of the lattice model: a) diffusion; b) rotation (free monomers only); c) formation of bonds between cells and aggregates leading to a free patch becoming occupied; d) formation of cell-mediated bonds between two aggregates.

In chapter 3, we studied the dynamics of a 3D system of monomers and cells through a lattice model where every aggregate occupied one lattice space, neglecting aggregate shape and patch correlations. In this chapter, we study a lattice model where these correlations are accounted for. For simplicity, the term "aggregate" will include monomers. The size of an aggregate is defined as the number of monomers in it; free monomers are aggregates of size one.

Monomers occupy a lattice space and move by a sequence of random hops to their nearest neighbors (see Fig. 4.1 a)). The hopping rate is related to the translational diffusion coefficient D_m. A lattice space cannot be occupied by more than one monomer. The density of monomers n_m is defined as the ratio of lattice spaces occupied by monomers at $t = 0$. Monomers have a number f of patches on their surface given by the coordination number of the underlying lattice. f is the maximum number of bonds they can form. A patch can be free and form no bond or it can be occupied and form an irreversible bond to a cell. A patch cannot be occupied by more than one cell. Each patch points to one of the nearest neighbors of the monomer, which undergoes rigid rotations with a rate related to the rotational diffusion coefficient

D_r (see Fig. 4.1 b)).
As in the previous chapters, there is a second species, the cells. Cells occupy a lattice space and hop with a rate related to their diffusion coefficient D_c. A lattice space can be occupied by at most one cell. The density of cells n_c is defined as the ratio of lattice spaces occupied by cells at $t = 0$. Cells form irreversible bonds to patches. By forming a bond to a maximum of two patches, they mediate bonds between monomers. If a monomer and cell are adjacent and the patch of the monomer pointing towards the cell is free, then it is possible for one to hop to the lattice space occupied by the other. If so, the patch of the monomer which pointed towards the cell becomes occupied (see Fig. 4.1 c)).
When a monomer is adjacent to another monomer, the two form an irreversible cell-mediated bond if the two patches that point to one another include one free and one occupied patch (see Fig. 4.1 d)). Cell-mediated bonds between free monomers can occur after a hop or a rotation and results in a dimer. We neglect the rotation of aggregates of size larger than one. An aggregate of size S hops with a rate related to the diffusion coefficient D_m^S, such that all monomers that belong to it hop in the same direction. An aggregate may not hop if it is not possible for a monomer that belongs to it to hop, i.e when the adjacent lattice space is occupied by another monomer or occupied by a cell and the patch that points to it is occupied.
Unlike in the model discussed in chapter 3, aggregates may not be tree-like. Let S be the size of an aggregate, F and O be its number of free and occupied patches, respectively. Since for every cell-mediated bond an occupied and a free patch are used,

$$O + F = Sf - 2N_{bonds}, \tag{4.1}$$

where N_{bonds} is the number of cell-mediated bonds formed between monomers belonging to the aggregate. N_{bonds} can be split into two contributions,

$$N_{bonds} = S - 1 + N_L, \tag{4.2}$$

where $S - 1$ is the number of bonds in a tree-like aggregate and N_L is the number of redundant bonds, from which result loops. Combining eqs. (4.1) and (4.2), we obtain

$$O + F = S(f - 2) + 2 - 2N_L, \tag{4.3}$$

which is the general form of eq. (3.5) for any aggregate.
We measured the average size of the aggregates $\langle S \rangle(t)$ as a function of time defined as

$$\langle S \rangle = \frac{N}{N_{agg}}, \tag{4.4}$$

where N is the number of free monomers at $t = 0$ and $N_{agg}(t)$ is the number of aggregates as a function of time. As all monomers are free at $t = 0$, $N_{agg}(0) = N$. We have also measured the size $S_{max}(t)$ of the largest aggregate as a function of time, and the bond probability p_b, defined as the probability that a patch forms a cell-mediated bond with a second patch as a function of time. To characterize the shape of aggregates, we measure the fraction of all bonds which are redundant n_L.
All monomers and cells start free. Let C be the number of cells at $t = 0$. We define ϕ as the ratio of cells to patches,

$$\phi = \frac{C}{Nf}. \tag{4.5}$$

An aggregate of size S will diffuse with the coefficient D_m^S. Since time can be rescaled, the dynamics does not depend on the absolute value of the diffusion coefficients, but on their ratio. We define Δ as the ratio of cell and free monomer diffusion coefficients:

$$\Delta = \frac{D_c}{D_m^1}. \tag{4.6}$$

Henceforth, we will rescale time such that $D_m^1 = 1$. We assume the timescale of monomer rotation is of the same order of the timescale of monomer diffusion and set

$$D_r = D_m^1 = 1. \tag{4.7}$$

While the model is defined for a generic D_m^S, here only the limit where only free monomers diffuse was studied (section 4.2).

4.1 Computational methods

In chapter 3, the algorithm used was rejection-based in the sense that it could attempt an event that is not successful, e.g. a cell attempting to hop to a lattice space already occupied by a cell. While the correct time evolution is obtained and its implementation is simpler, the rejection-based algorithm is computationally inefficient. In the present chapter, simulations are performed with the rejection-free kinetic Monte Carlo method [24, 25].

Cells hop with rate q_c. We consider diffusion to be isotropic and so the rate of hopping in a certain direction q_c' is

$$q_c' = \frac{q_c}{z}, \tag{4.8}$$

where z is the coordination number of the underlying lattice. Aggregates of size S hop with rate $q_m'^S$. Free monomers rotate along a certain axis with rate q_r'. A list containing all possible events (i.e. all possible hops and rotations) is updated at every time step. The next event is chosen from this list with a probability proportional to its rate. Choosing from the list ensures no events are rejected and considerably reduces the computational demands when compared to the rejection-based algorithm in chapter 3.

We consider events to be uncorrelated in space and time and so the total rate of events Q is the sum of the rates of all events in the list. The time between hops Δt is a random variable described by an exponential distribution and is generated by

$$\Delta t = -\frac{\log(\psi)}{Q}, \tag{4.9}$$

where $\psi \in]0, 1]$ is a uniformly generated random variable. This method of incrementing the simulation clock preserves the correct time evolution.

The rates q_c' and $q_m'^S$ are obtained with an argument similar to chapter 3. For any dimension, we obtain

$$q_c' = \frac{D_c}{\Delta x^2}, \tag{4.10}$$

$$q_m'^S = \frac{D_m^S}{\Delta x^2}, \tag{4.11}$$

where D_c and D_m^S are the diffusion coefficients of cells and aggregates of size S respectively, and Δx is the lattice constant. Simulations were performed on a 3D cubic lattice of linear length L_{box} using periodic boundary conditions. To keep consistency with the simulations in chapter 3, we set $\Delta x = \sqrt{6}$

and rescale time such that $q_m'^1 = D_m^1/6 = 1/6$. As we study the limit $n_m \ll 1$, the discretization of the lattice does not significantly influence the results. It is assumed that the the timescale of rotation of monomers is of the same order as the timescale of diffusion of monomers and so we set

$$q_r' = q_m'^1. \tag{4.12}$$

All simulations were for $f = 6$. A monomer is thus described by a three-dimensional position vector $\vec{x}$ and a six-dimensional configuration vector $\vec{o}$ related to the occupancy of the patches. A simple way to reduce the memory usage of the event list is mapping both vectors to integers. The position vector $\vec{x}$

$$\vec{x} = \{x_1, x_2, x_3\}, \tag{4.13}$$

is mapped to an integer X (where x_1, x_2, x_3 are integers),

$$X = x_1 + x_2 L_{box} + x_3 L_{box}^2. \tag{4.14}$$

The reverse mapping is

$$x_1 = \left(X \% L_{box}^2\right) \% L_{box}, \tag{4.15}$$
$$x_2 = \left(X \% L_{box}^2\right) // L_{box}, \tag{4.16}$$
$$x_3 = X // L_{box}^2, \tag{4.17}$$

where the functions $a\%b$ and $a//b$ are the remainder of the division of a by b and the integer division of a by b, respectively. This transformation is a one-to-one correspondence as $0 \leq x_1, x_2, x_3 < L_{box}$. The configuration vector $\vec{o}$ is written explicitly as

$$\vec{o} = \{o_1, o_2, o_3, o_4, o_5, o_6\}, \tag{4.18}$$

where the coordinates o_i are Booleans with 1 indicating an occupied patch and 0 a free patch. The variable i indexes the direction the patch is facing. In the same style as with $\vec{x}$, $\vec{o}$ is transformed to an integer O,

$$O = \sum_{i=1}^{6} o_i 2^{i-1}, \tag{4.19}$$

with the inverse transformation given iteratively,

$$\begin{cases} o_6 & = O // 2^5 \quad \text{(4.20a)} \\ o_i & = \left(o_{i+1} \% 2^i\right) // 2^{i-1}\ ,\ 1 \leq i \leq 5. \quad \text{(4.20b)} \end{cases}$$

4.2 Diffusion of only free monomers

In section 3.3, we studied the limit where diffusion of aggregates of size larger than one can be neglected in the timescale of free monomer diffusion. We therefore referred to aggregates of size larger than one as "aggregates" and

$$D_m^S = \delta_{S,1}, \tag{4.21}$$

where $\delta_{i,j}$ is the Kroenecker delta.

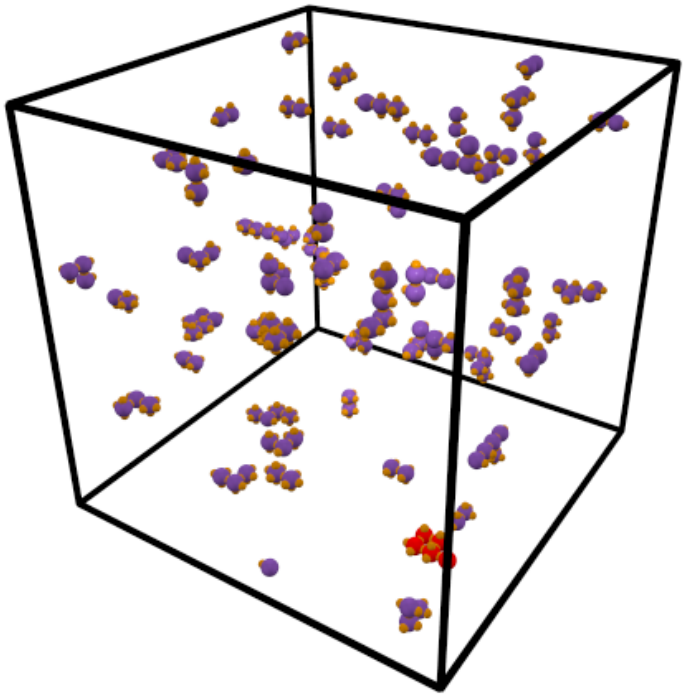

Figure 4.2: Snapshot of a simulation. Monomers are in purple and cells in orange. The largest aggregate is shown in red.

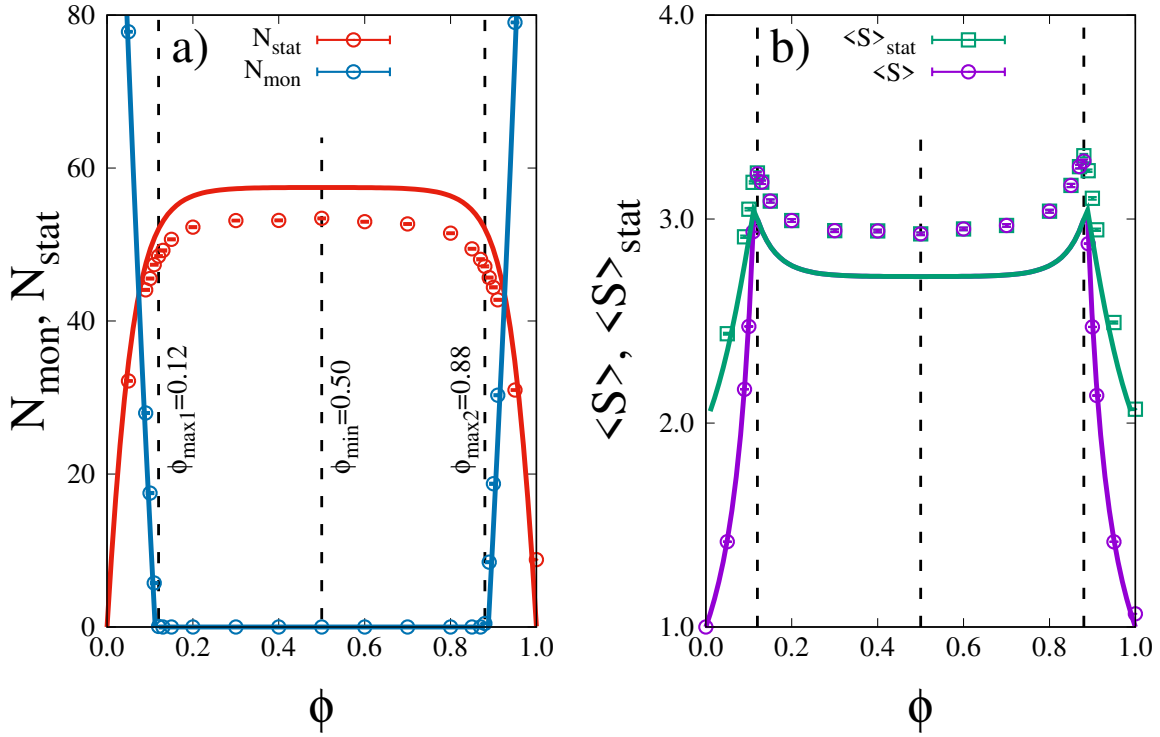

Figure 4.3: Comparison of simulations (points) with the mean-field theory of section 3.3 in the asymptotic limit. Simulation parameters are $L_{box} = 25$, $n_m = 0.01$, $\Delta = 1000$. Simulations were averaged over 500 samples. a) Number of free monomers N_{mon} and aggregates of size larger than one N_{stat}; b) average size of aggregates and monomers $\langle S \rangle$ and average size of the aggregates $\langle S \rangle_{stat}$.

A snapshot of a simulation can be found in Fig. 4.3. When cells are much faster than monomers ($\Delta \to \infty$), the dynamics separate into two regimes. First is the cell regime, in which only cells diffuse. All cells form one bond in the cell regime. Afterwards is the monomer regime where only free monomers

diffuse.

We measured the average size of aggregates and monomers $\langle S \rangle$ and the average size of aggregates $\langle S \rangle_{stat}$ defined as

$$\langle S \rangle_{stat} = \frac{N - N_{mon}}{N_{stat}}, \tag{4.22}$$

where N_{mon} is the number of free monomers. It was found that both the asymptotic values of $\langle S \rangle$ and $\langle S \rangle_{stat}$ exhibited bimodal shapes when mapped as function of ϕ. These bimodal shapes arose in the point-like model of chapter 3 due to the form of the distribution of occupied patches after the cell regime. A mean-field theory was developed which captured the physics. Figure 4.3 shows the bimodal shape is present in the model introduced in this chapter. Figure 4.4 b) shows that the bimodal shape is not a finite-size effect, but caused by the mechanism discussed in chapter 3.

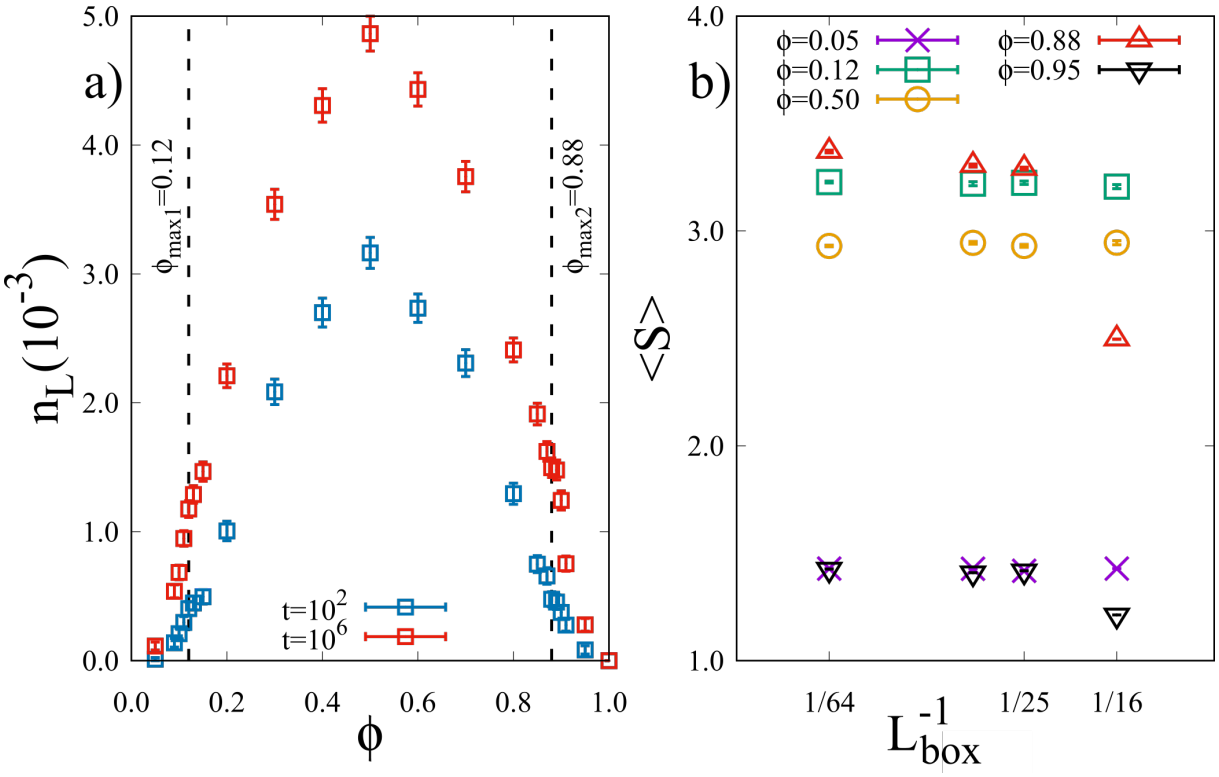

Figure 4.4: a) Fraction of bonds which are redundant n_L as a function of ϕ for two values of time. Simulations were averaged over 2500 samples. Dashed lines represent the values of ϕ which maximize $\langle S \rangle$ and $\langle S \rangle_{stat}$. b) Average size of aggregates $\langle S \rangle$ as function of L_{box}^{-1} for different value of ϕ. Simulation parameters are $n_m = 0.01$, $\Delta = 10^3$. Simulations were averaged over $\{1000, 500, 250, 100\}$ samples for $L_{box} = \{16, 25, 32, 64\}$, respectively.

To quantify the inter-connectivity of the aggregates, we measure the fraction of bonds which are redundant n_L. In Fig. 4.4 a), it can be seen that $n_L < 1\%$ for all values of ϕ. Because the average size of the aggregates is at most ≈ 3.25, it is noteworthy to mention that only aggregates of size larger than three may exhibit loops in a cubic lattice, which partially explains the low values of n_L. Also relevant is the fact that redundant bonds occur when a free monomer forms more than one bond to an aggregate in the same time step, which is a much rarer event that the formation of a single bond. Larger values of $\langle S \rangle_{stat}$ increase the probability that a free monomer is adjacent to two or more monomers belonging to the same aggregate. Despite $\langle S \rangle_{stat}$ being maximized for $\phi = \{0.12, 0.88\} \pm 0.01$, no maxima are present in n_L at those values of ϕ. The variation in $\langle S \rangle_{stat}$ is too small to play a decisive role in n_L. The formation of two or more bonds requires more than just adjacency of multiple monomers, it also requires that the patches between monomers form free/occupied pairs. If we discard the effect of $\langle S \rangle_{stat}$, the probability of a free

monomer forming a second cell-mediated bond after forming a first link is maximized for $\phi = 0.5$, in which the total number of free and occupied patches is equal.

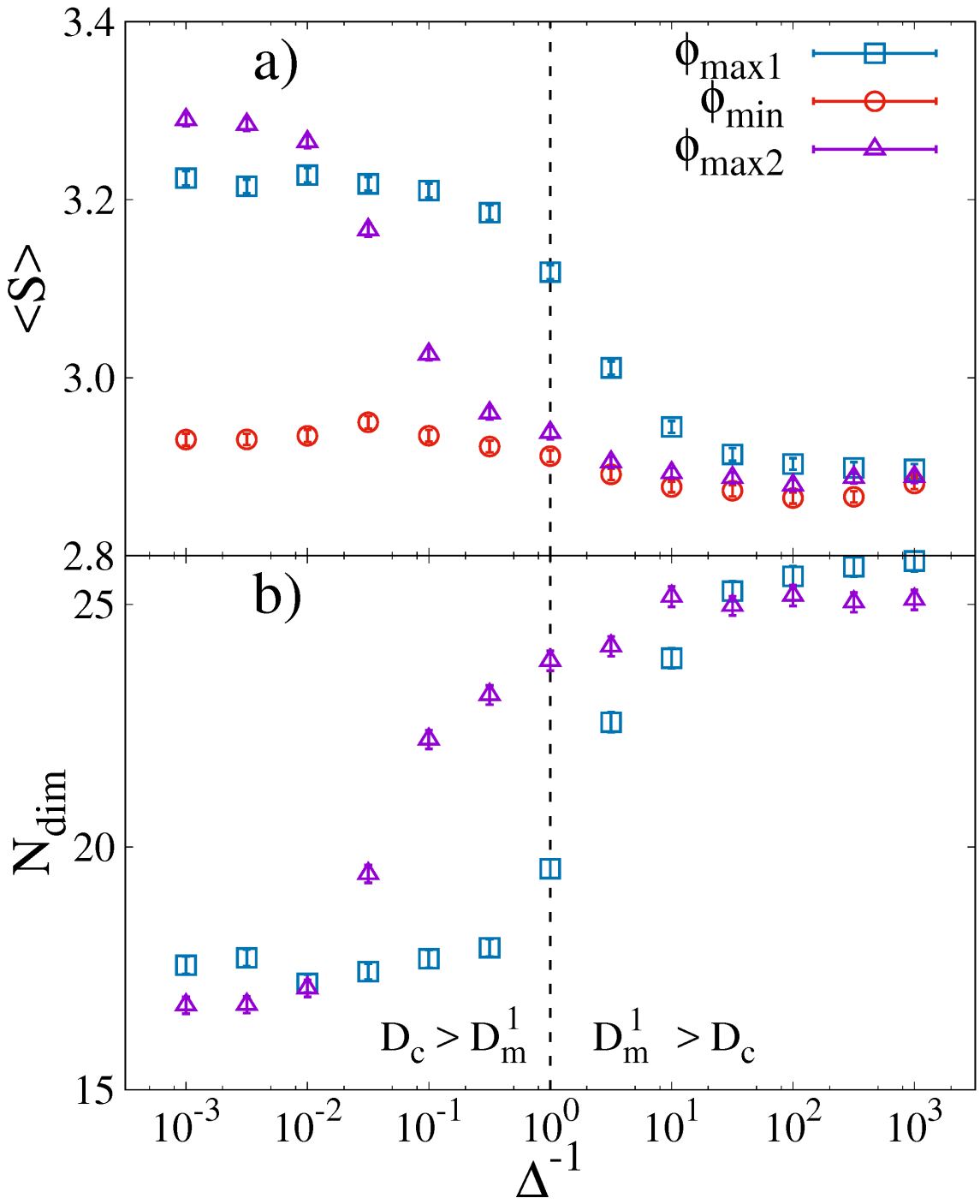

Figure 4.5: Dependency on ratio of cell and monomer diffusion coefficient Δ in the asymptotic limit of a) the height of the maxima and minimum in the average size of aggregates $\langle S \rangle$; b) the number of dimers N_{dim}. Squares correspond to $\phi_{max1} = 0.12$ and triangles to $\phi_{max2} = 0.88$. Dashed line separates the region of parameters in which cells diffuse faster than monomers (left) from the region in which monomers diffuse faster than cells (right). Simulations were performed on a system of lateral size $L_{box} = 25$, monomer density of $n_m = 0.01$, and averaged over 500 samples.

Until now, we have considered the case of cell diffusion much faster than monomer diffusion $\Delta \gg 1$. For a finite Δ, the timescale of cell diffusion is no longer separable from that of monomer diffusion,

meaning cells can form a second bond before all cells form a first bond. While the values of ϕ_{max1}, ϕ_{min} and ϕ_{max2} do not change with Δ, $\langle S \rangle$ does. In the asymptotic limit and $\Delta \to 0$, it was found that there is an initial regime in which larger values of ϕ increase $\langle S \rangle$, evolving to a plateau in which $\langle S \rangle$ is constant with ϕ (up to the largest measured value of $\phi = 1.0$). In particular, the maxima disappear. Figure 4.5 displays the effect of Δ in the maxima and minimum of $\langle S \rangle$. The order of magnitude of the value of Δ at which the maximum for ϕ_{max1} disappears differs from that of ϕ_{max2}.

As shown in chapter 3, the maxima are due to low rates of formation of bonds between monomers with only free or occupied patches, which lowers the number of dimers when compared to ϕ_{min}. The disappearing of the maxima is thus associated with an increased number of dimers, as seen in Fig. 4.5 b). Because some but not all cells form bonds to patches, a system with finite Δ behaves like a system with $\Delta \to \infty$ but with an effective value of ϕ that is lower, provided there are more than enough cells for all monomers to form cell-mediated bonds. For ϕ_{max2}, this lower effective ϕ causes more monomers to have both free and occupied patches which increases the number of dimers, resulting in lower $\langle S \rangle$ when $\Delta \lesssim 10^2$. For ϕ_{min}, the effective reduction in ϕ does not change $\langle S \rangle$ much as the number of monomers with both free and occupied patches does not change much.

The mechanism that increases the number of dimers for ϕ_{max1} is different than for ϕ_{max2} because there are barely enough cells for all monomers to form cell-mediated bonds and the equivalence with the case $\Delta \to \infty$ and lower effective ϕ is not valid. While monomers do not have enough occupied patches for all of them to form cell-mediated bonds when their diffusion starts to be relevant around $\Delta \approx 10^2$, there are still enough cells in total and we must simply wait longer times to retain the maximum.Therefore, the mechanism for the increase in the number of dimers in ϕ_{max1} is different and visible only when $\Delta \lesssim 1$. When $\Delta \to 0$, the relevant timescale is given by the diffusion of monomers. For $\Delta \lesssim 1$, cells are mainly static, and monomers are responsible for dimer formation (through formation of bonds with static linkers) as seen in Fig. 4.5 b). The longer timescale of linker diffusion results on a later arrival to the empty patches of already static aggregates (dimers), minimizing further aggregation.

To finish this section, we verify that varying monomer density n_m does not suppress the bimodal shape of $\langle S \rangle$ when $n_m \ll 1$ and $\Delta \to \infty$. Figure 4.6 shows the asymptotic height of the maxima and minimum of $\langle S \rangle$ as function of n_m and the inset shows their corresponding value of ϕ. It was found that, when $n_m \ll 1$, the height of the maxima and minimum scale linearly with n_m,

$$\langle S \rangle \propto n_m \ , \ n_m \ll 1. \tag{4.23}$$

Extrapolating to find the height of the maxima in the limit $n_m \to 0$, it is found that they are equal. In this limit, spatial correlations are non-existent and $\langle S \rangle$ is symmetrical, as predicted by the analysis of chapter 3. Spatial correlations play a larger role in systems with larger value of n_m, e.g. two aggregates merging due to a monomer forming a bridge between them. In these systems, the curve $\langle S \rangle(\phi)$ has an asymmetry.

The linear fits for $\langle S \rangle(\phi_{min})$ and $\langle S \rangle(\phi_{max1})$ intersect for $n_m \approx 0.48$. For $n_m > 0.48$, the bimodal shape of $\langle S \rangle$ is not present. This conclusion is consistent with the results seen in the inset of Fig. 4.6, as the value of ϕ_{min} approaches the value of ϕ_{max1}, which remains constant with n_m. Simulations were performed for $n_m = 0.55$ and no maximum was found in the range $\phi \in [0.11, 0.13]$.

At values of n_m large enough such that $n_m + n_c$ is comparable to 1, the dynamics are effected by the discretization, e.g. cubic vs. hexagonal lattice. Such dependency on the underlying lattice is unphysical as the on-lattice models of this chapter and of chapter 3 are simplifications of a continuous system. The limit in which the results of our on-lattice models are most realistic is the limit $n_m \to 0$, where

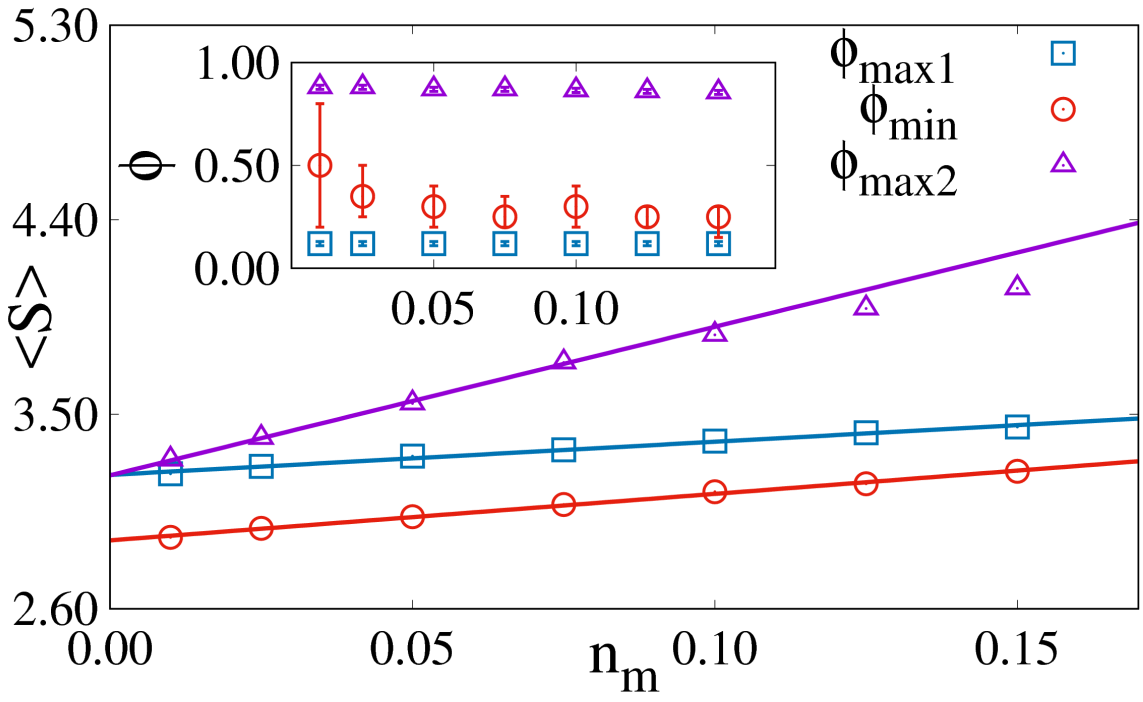

Figure 4.6: Dependency on monomer density n_m of the maxima and minimum in the asymptotic $\langle S \rangle$. Lines were obtained with minimum square fits. Inset shows the value of ratio of cells to patches ϕ at which the maxima and minimum were found. Squares refer to the smallest local maximum found, circles to the local minimum, and triangles to the largest local maximum. Simulations parameters are $L_{box} = 25$, and $\Delta = 10^3$. Results were averaged over 500 samples.

the average distance between aggregates is much larger than the average distance between monomers belonging to the same aggregate; a more detailed study of the dependency on n_m and the associated discretization effects will not be presented.

Conclusion

The central problem studied here is the aggregation process of self-assembled scaffolds composed of chitosan particles linked together by cells, which we modeled with patchy particles. We started with a simplified analysis, increasing the complexity stepwise: in chapter 1, we developed mean-field rate equations, while correlations between aggregates and patches were introduced in chapters 3 and 4, respectively. This gradual addition of features allowed isolated studies, resulting in a deeper understanding of how aggregation depends on each model (e.g. diffusion and concentration of species).

Cells adhere to one another to form tissues. In chapter 2, we compared two models for scaffold self-assembly focused on the dynamics of the cells, a first in which cells can form bonds to one another and a second where they cannot. It was found that suppressing this natural behavior resulted in larger, more interconnected scaffolds that grew faster, which is of great practical interest. A large, mechanically resilient scaffold is required for the growth of healthy, macroscopic tissue. Furthermore, the quicker the scaffold assembles, the less likely it is for the assembly process to be effected by the natural bioactivity of the surrounding environment. Decreasing the formation time also increases the quality of life of the treated patients and decreases medical expenses. For the remainder of the work, we focused on the model with suppressed cell-cell bonds, for which we obtained multiple analytical and numerical results, such as the distribution of cells and the probability that a patch forms a cell-mediated bond to another patch. An application of mean-field percolation theory bridges the gap between cell dynamics and scaffold structure, predicting the formation of a gel. It was found that there is a value of the ratio of cells to particles that optimizes scaffold growth.

In chapter 3, we introduced spatial correlations between aggregates through a lattice model, which we solved numerically through a Monte Carlo algorithm. The lattice model considered aggregates to be point-like and tree-like. We first studied the limit in which the diffusion coefficient of aggregates was independent of their size. An interval of the ratio of cells to particles was found such that a giant aggregate that includes all particles forms, in agreement with some simple calculations. We have also obtained the functional form of the size distribution of aggregates for some intervals of the ratio of cells to particles. We then studied the limit in which there is a separation of timescales between the diffusion of free monomers and the diffusion of aggregates of size two or more. It was found that the average size of aggregates exhibits a bimodal shape as a function of the ratio of cells to particles with two optimal values in the asymptotic limit for a high value of the ratio of the diffusion coefficients of cells and particles. This shape is preceded by a regime in which there is only one optimal value. The proposed mechanism involving the suppression of bonds between a portion of the monomers controlled by the occupied patch distribution was verified with an analytical treatment and simulations.

Finally, in chapter 4, we introduced aggregate shape and patch correlations in the limit where the timescale of the diffusion of free monomers is separate from the diffusion of aggregates of size two or more. Simulations were performed with the more efficient kinetic Monte Carlo algorithm. In the limit where the diffusion of cells is much faster than the diffusion of free monomers, a bimodal shape was

found for the average size of aggregates, similarly to chapter 3, allowing us to conclude aggregate shape is not a key feature of the mechanism. It was found there is an optimum value of the ratio of cells to particles for the fraction of loops which coincides with the value which maximizes scaffold growth, explained through the distribution of occupied patches. It was further found that the maxima in the average size of aggregates is not relevant for the fraction of loops. The possibility of indirectly tuning the fraction of loops through the ratio of cells to particles allows the tuning of the porosity and mechanical rigidity of the scaffold, for which there are strict requirements.

We studied the effect of the ratio of cell and monomer diffusion coefficients, having found that the maxima in the average size of aggregates disappear when monomers are much faster than cells. The two maxima disappear at different diffusion timescales due to two different mechanisms; one involving an effective reduction in the ratio of cells to particles and one involving a reduced rate of formation of bonds between cells and dimers. Both mechanisms result in an increased number of dimers in the asymptotic limit. We concluded with a study of the density of monomers, where we show that both the values of the ratio of cells to particles corresponding to the maxima and their height depend on the density of monomers. We obtain a linear dependency of the height of the maxima valid for low densities, which is the limit where the lattice model is most realistic.

Even though the motivation for this study is in scaffold formation, these results are relevant for any system that exhibits aggregation mediated by a second species and it is of interest to practitioners to understand how experimental conditions and timescales can affect targeted structures. Extensions of the work developed can include a study of the lattice model of chapter 4 for a generic relation between aggregate size and diffusion coefficient. The diffusivity of clusters has been studied extensively both for liquids [26] and for adsorption on surfaces [27]. Furthermore, it is of interest to compare the results of cell-mediated aggregation with the work of P. Meakin, which contains numerous results involving the size distribution in the simple one-species aggregation model [28]. Of high interest to the motivation is the measurement of the porosity and mechanical strength of the self-assembled structures. Working in tandem with Molecular Dynamics studies, more realistic rates for bond breaking can be introduced such as to model the self-assembly of scaffolds in e.g. sheared fluids.

Bibliography

[1] C. A. Custódio, M. T. Cerqueira, A. P. Marques, R. L. Reis, and J. F. Mano. Cell selective chitosan microparticles as injectable cell carriers for tissue regeneration. *Biomaterials*, 43:23 – 31, 2015.

[2] AnhVu Do, Behnoush Khorsand, Sean M. Geary, and Aliasger K. Salem. 3d printing of scaffolds for tissue regeneration applications. *Advanced Healthcare Materials*, 4(12):1742–1762, 2015.

[3] Dietmar W. Hutmacher. Scaffolds in tissue engineering bone and cartilage. In D.F. Williams, editor, *The Biomaterials: Silver Jubilee Compendium*, pages 175 – 189. Elsevier Science, Oxford, 2000.

[4] Susmita Bose, Sahar Vahabzadeh, and Amit Bandyopadhyay. Bone tissue engineering using 3d printing. *Materials Today*, 16(12):496 – 504, 2013.

[5] Christian Frantz, Kathleen M. Stewart, and Valerie M. Weaver. The extracellular matrix at a glance. *Journal of Cell Science*, 123(24):4195–4200, 2010.

[6] S. J. Hollister. Porous scaffold design for tissue engineering. *Nature Materials*, 4:518–524, 2005.

[7] António J. Salgado, Olga P. Coutinho, and Rui L. Reis. Bone tissue engineering: State of the art and future trends. *Macromolecular Bioscience*, 4(8):743–765, 2004.

[8] Shoufeng Yang, Kah Fai Leong, Zhaohui Du, and Chee-Kai Chua. The design of scaffolds for use in tissue engineering. part i. traditional factors. *Tissue Engineering*, 7(6):679–689, 2001.

[9] Daniel Druecke, Stefan Langer, Evert Lamme, Jeroen Pieper, Marija Ugarkovic, Hans Ulrich Steinau, and Heinz Herbert Homann. Neovascularization of poly(ether ester) block-copolymer scaffolds in vivo: Long-term investigations using intravital fluorescent microscopy. *Journal of Biomedical Materials Research Part A*, 68A(1):10–18, 2003.

[10] Amin Bandyopadhyay, Susmita Bose, and Suman Das. 3d printing of biomaterials. *MRS Bulletin*, 40(2):108–115, 2015.

[11] Kimiko Takahashi, Yoshio Sawasaki, Jun-Ichi Hata, Kiyoshi Mukai, and Tamotsu Goto. Spontaneous transformation and immortalization of human endothelial cells. *In Vitro Cellular & Developmental Biology*, 26(3):265–274, Mar 1990.

[12] GI Bell. Models for the specific adhesion of cells to cells. *Science*, 200(4342):618–627, 1978.

[13] B. A. Lindquist, R. B. Jadrich, D. J. Milliron, and T. M. Truskett. On the formation of equilibrium gels via a macroscopic bond limitation. *J. Chem. Phys.*, 145:074906, 2016.

[14] Ovijit Chaudhuri, Luo Gu, Max Darnell, Darinka Klumpers, Sidi A. Bencherif, James C. Weaver, Nathaniel Huebsch, and David J. Mooney. Substrate stress relaxation regulates cell spreading. *Nature Communications*, 6, 2015.

[15] Oleg R. Musin. The kissing problem in three dimensions. *Discrete & Computational Geometry*, 35(3):375–384, 2006.

[16] J. K. G. Dhont. *An introduction to dynamics of colloids*. Elsevier, 1996.

[17] Pavel L. Krapivsky, Sidney Redner, and Eli Ben-Naim. *A Kinetic View of Statistical Physics*. Cambridge University Press, 2010.

[18] S. Chandrasekhar. Stochastic problems in physics and astronomy. *Rev. Mod. Phys.*, 15(1), 1943.

[19] John T. Edward. Molecular volumes and the Stokes-Einstein equation. *Journal of Chemical Education*, 47(4):261, 1970.

[20] A. Cadilhe, N. A. M. Araújo, and V. Privman. Random sequential adsorption: from continuum to lattice and pre-patterned substrates. *Journal of Physics: Condensed Matter*, 19(6), 2007.

[21] Abbas Ali Saberi. Growth models on the Bethe lattice. *EPL (Europhysics Letters)*, 103(1):10005, 2013.

[22] M. E. J. Newman. *Networks: an introduction*. Oxford University Press, 2010.

[23] Paul J. Flory. Molecular size distribution in three dimensional polymers. i. gelation. *Journal of the American Chemical Society*, 63(11):3083–3090, 1941.

[24] A. B. Bortz, M. H. Kalos, and J. L. Lebowitz. A new algorithm for Monte Carlo simulation of Ising spin systems. *Journal of Computational Physics*, 17(1):10, 1975.

[25] Corbett C. Battaile. The kinetic Monte Carlo method: Foundation, implementation, and application. *Computer Methods in Applied Mechanics and Engineering*, 197(41-42):3386–3398, 2008.

[26] E. L. Cussler. Cluster diffusion in liquids. *AIChE Journal*, 26(1):43–51, 1980.

[27] Clinton DeW. Van Siclen. Single jump mechanisms for large cluster diffusion on metal surfaces. *Phys. Rev. Lett.*, 75(8):1574–1577, Aug 1995.

[28] Paul Meakin, Tamás Vicsek, and Fereydoon Family. Dynamic cluster-size distribution in cluster-cluster aggregation: Effects of cluster diffusivity. *Physical review. B, Condensed matter*, 31:564–569, 1985.